

Observation of $\Lambda_c^+ \rightarrow \Lambda a_0(980)^+$ and Evidence for $\Sigma(1380)^+$ in $\Lambda_c^+ \rightarrow \Lambda \pi^+ \eta$

M. Ablikim¹, M. N. Achasov^{4,c}, P. Adlarson⁷⁵, O. Afedulidis³, X. C. Ai⁸⁰, R. Aliberti³⁵, A. Amoroso^{74A,74C}, Q. An^{71,58,a}, Y. Bai⁵⁷, O. Bakina³⁶, I. Balossino^{29A}, Y. Ban^{46,h}, H.-R. Bao⁶³, V. Batozskaya^{1,44}, K. Begzsuren³², N. Berger³⁵, M. Berlowski⁴⁴, M. Bertani^{28A}, D. Bettone^{29A}, F. Bianchi^{74A,74C}, E. Bianco^{74A,74C}, A. Bortone^{74A,74C}, I. Boyko³⁶, R. A. Briere⁵, A. Brueggemann⁶⁸, H. Cai⁷⁶, X. Cai^{1,58}, A. Calcaterra^{28A}, G. F. Cao^{1,63}, N. Cao^{1,63}, S. A. Cetin^{62A}, J. F. Chang^{1,58}, G. R. Che⁴³, G. Chelkov^{36,b}, C. Chen⁴³, C. H. Chen⁹, Chao Chen⁵⁵, G. Chen¹, H. S. Chen^{1,63}, H. Y. Chen²⁰, M. L. Chen^{1,58,63}, S. J. Chen⁴², S. L. Chen⁴⁵, S. M. Chen⁶¹, T. Chen^{1,63}, X. R. Chen^{31,63}, X. T. Chen^{1,63}, Y. B. Chen^{1,58}, Y. Q. Chen³⁴, Z. J. Chen^{25,i}, Z. Y. Chen^{1,63}, S. K. Choi^{10A}, G. Cibinetto^{29A}, F. Cossio^{74C}, J. J. Cui⁵⁰, H. L. Dai^{1,58}, J. P. Dai⁷⁸, A. Dbeysi¹⁸, R. E. de Boer³, D. Dedovich³⁶, C. Q. Deng⁷², Z. Y. Deng¹, A. Denig³⁵, I. Denysenko³⁶, M. Destefanis^{74A,74C}, F. De Mori^{74A,74C}, B. Ding^{66,1}, X. X. Ding^{46,h}, Y. Ding⁴⁰, Y. Ding³⁴, J. Dong^{1,58}, L. Y. Dong^{1,63}, M. Y. Dong^{1,58,63}, X. Dong⁷⁶, M. C. Du¹, S. X. Du⁸⁰, Y. Y. Duan⁵⁵, Z. H. Duan⁴², P. Egorov^{36,b}, Y. H. Fan⁴⁵, J. Fang⁵⁹, J. Fang^{1,58}, S. S. Fang^{1,63}, W. X. Fang¹, Y. Fang¹, Y. Q. Fang^{1,58}, R. Farinelli^{29A}, L. Fava^{74B,74C}, F. Feldbauer³, G. Felici^{28A}, C. Q. Feng^{71,58}, J. H. Feng⁵⁹, Y. T. Feng^{71,58}, M. Fritsch³, C. D. Fu¹, J. L. Fu⁶³, Y. W. Fu^{1,63}, H. Gao⁶³, X. B. Gao⁴¹, Y. N. Gao^{46,h}, Yang Gao^{71,58}, S. Garbolino^{74C}, I. Garzia^{29A,29B}, L. Ge⁸⁰, P. T. Ge⁷⁶, Z. W. Ge⁴², C. Geng⁵⁹, E. M. Gersabeck⁶⁷, A. Gilman⁶⁹, K. Goetzen¹³, L. Gong⁴⁰, W. X. Gong^{1,58}, W. Gradl³⁵, S. Gramigna^{29A,29B}, M. Greco^{74A,74C}, M. H. Gu^{1,58}, Y. T. Gu¹⁵, C. Y. Guan^{1,63}, A. Q. Guo^{31,63}, L. B. Guo⁴¹, M. J. Guo⁵⁰, R. P. Guo⁴⁹, Y. P. Guo^{12,g}, A. Guskov^{36,b}, J. Gutierrez²⁷, K. L. Han⁶³, T. T. Han¹, F. Hanisch³, X. Q. Hao¹⁹, F. A. Harris⁶⁵, K. K. He⁵⁵, K. L. He^{1,63}, F. H. Heinsius³, C. H. Heinz³⁵, Y. K. Heng^{1,58,63}, C. Herold⁶⁰, T. Holtmann³, P. C. Hong³⁴, G. Y. Hou^{1,63}, X. T. Hou^{1,63}, Y. R. Hou⁶³, Z. L. Hou¹, B. Y. Hu⁵⁹, H. M. Hu^{1,63}, J. F. Hu^{56,j}, S. L. Hu^{12,g}, T. Hu^{1,58,63}, Y. Hu¹, G. S. Huang^{71,58}, K. X. Huang⁵⁹, L. Q. Huang^{31,63}, X. T. Huang⁵⁰, Y. P. Huang¹, Y. S. Huang⁵⁹, T. Hussain⁷³, F. Hölzken³, N. Hüskens³⁵, N. in der Wiesche⁶⁸, J. Jackson²⁷, S. Janchiv³², J. H. Jeong^{10A}, Q. Ji¹, Q. P. Ji¹⁹, W. Ji^{1,63}, X. B. Ji^{1,63}, X. L. Ji^{1,58}, Y. Y. Ji⁵⁰, X. Q. Jia⁵⁰, Z. K. Jia^{71,58}, D. Jiang^{1,63}, H. B. Jiang⁷⁶, P. C. Jiang^{46,h}, S. S. Jiang³⁹, T. J. Jiang¹⁶, X. S. Jiang^{1,58,63}, Y. Jiang⁶³, J. B. Jiao⁵⁰, J. K. Jiao³⁴, Z. Jiao²³, S. Jin⁴², Y. Jin⁶⁶, M. Q. Jing^{1,63}, X. M. Jing⁶³, T. Johansson⁷⁵, S. Kabana³³, N. Kalantar-Nayestanaki⁶⁴, X. L. Kang⁹, X. S. Kang⁴⁰, M. Kavatsyuk⁶⁴, B. C. Ke⁸⁰, V. Khachatryan²⁷, A. Khoukaz⁶⁸, R. Kiuchi¹, O. B. Kolcu^{62A}, B. Kopf³, M. Kuessner³, X. Kui^{1,63}, N. Kumar²⁶, A. Kupsc^{44,75}, W. Kühn³⁷, J. J. Lane⁶⁷, P. Larin¹⁸, L. Lavezzi^{74A,74C}, T. T. Lei^{71,58}, Z. H. Lei^{71,58}, M. Lellmann³⁵, T. Lenz³⁵, C. Li⁴³, C. Li⁴⁷, C. H. Li³⁹, Cheng Li^{71,58}, D. M. Li⁸⁰, F. Li^{1,58}, G. Li¹, H. B. Li^{1,63}, H. J. Li¹⁹, H. N. Li^{56,j}, Hui Li⁴³, J. R. Li⁶¹, J. S. Li⁵⁹, K. Li¹, L. J. Li^{1,63}, L. K. Li¹, Lei Li⁴⁸, M. H. Li⁴³, P. R. Li^{38,k,l}, Q. M. Li^{1,63}, Q. X. Li⁵⁰, R. Li^{17,31}, S. X. Li¹², T. Li⁵⁰, W. D. Li^{1,63}, W. G. Li^{1,a}, X. Li^{1,63}, X. H. Li^{71,58}, X. L. Li⁵⁰, X. Y. Li^{1,63}, X. Z. Li⁵⁹, Y. G. Li^{46,h}, Z. J. Li⁵⁹, Z. Y. Li⁷⁸, C. Liang⁴², H. Liang^{1,63}, H. Liang^{71,58}, Y. F. Liang⁵⁴, Y. T. Liang^{31,63}, G. R. Liao¹⁴, L. Z. Liao⁵⁰, Y. P. Liao^{1,63}, J. Libby²⁶, A. Limphirat⁶⁰, C. C. Lin⁵⁵, D. X. Lin^{31,63}, T. Lin¹, B. J. Liu¹, B. X. Liu⁷⁶, C. Liu³⁴, C. X. Liu¹, F. Liu¹, F. H. Liu⁵³, Feng Liu⁶, G. M. Liu^{56,j}, H. Liu^{38,k,l}, H. B. Liu¹⁵, H. H. Liu¹, H. M. Liu^{1,63}, Huihui Liu²¹, J. B. Liu^{71,58}, J. Y. Liu^{1,63}, K. Liu^{38,k,l}, K. Y. Liu⁴⁰, Ke Liu²², L. Liu^{71,58}, L. C. Liu⁴³, Lu Liu⁴³, M. H. Liu^{12,g}, P. L. Liu¹, Q. Liu⁶³, S. B. Liu^{71,58}, T. Liu^{12,g}, W. K. Liu⁴³, W. M. Liu^{71,58}, X. Liu^{38,k,l}, X. Liu³⁹, Y. Liu⁸⁰, Y. Liu^{38,k,l}, Y. B. Liu⁴³, Z. A. Liu^{1,58,63}, Z. D. Liu⁹, Z. Q. Liu⁵⁰, X. C. Lou^{1,58,63}, F. X. Lu⁵⁹, H. J. Lu²³, J. G. Lu^{1,58}, X. L. Lu¹, Y. Lu⁷, Y. P. Lu^{1,58}, Z. H. Lu^{1,63}, C. L. Luo⁴¹, J. R. Luo⁵⁹, M. X. Luo⁷⁹, T. Luo^{12,g}, X. L. Luo^{1,58}, X. R. Lyu⁶³, Y. F. Lyu⁴³, F. C. Ma⁴⁰, H. Ma⁷⁸, H. L. Ma¹, J. L. Ma^{1,63}, L. L. Ma⁵⁰, M. M. Ma^{1,63}, Q. M. Ma¹, R. Q. Ma^{1,63}, T. Ma^{71,58}, X. T. Ma^{1,63}, X. Y. Ma^{1,58}, Y. Ma^{46,h}, Y. M. Ma³¹, F. E. Maas¹⁸, M. Maggiora^{74A,74C}, S. Malde⁶⁹, Y. J. Mao^{46,h}, Z. P. Mao¹, S. Marcello^{74A,74C}, Z. X. Meng⁶⁶, J. G. Messchendorp^{13,64}, G. Mezzadri^{29A}, H. Miao^{1,63}, T. J. Min⁴², R. E. Mitchell²⁷, X. H. Mo^{1,58,63}, B. Moses²⁷, N. Yu. Muchnoi^{4,c}, J. Muskalla³⁵, Y. Nefedov³⁶, F. Nerling^{18,e}, L. S. Nie²⁰, I. B. Nikolaev^{4,c}, Z. Ning^{1,58}, S. Nisar^{11,m}, Q. L. Niu^{38,k,l}, W. D. Niu⁵⁵, Y. Niu⁵⁰, S. L. Olsen⁶³, Q. Ouyang^{1,58,63}, S. Pacetti^{28B,28C}, X. Pan⁵⁵, Y. Pan⁵⁷, A. Pathak³⁴, P. Patteri^{28A}, Y. P. Pei^{71,58}, M. Pelizaeus³, H. P. Peng^{71,58}, Y. Y. Peng^{38,k,l}, K. Peters^{13,e}, J. L. Ping⁴¹, R. G. Ping^{1,63}, S. Plura³⁵, V. Prasad³³, F. Z. Qi¹, H. Qi^{71,58}, H. R. Qi⁶¹, M. Qi⁴², T. Y. Qi^{12,g}, S. Qian^{1,58}, W. B. Qian⁶³, C. F. Qiao⁶³, X. K. Qiao⁸⁰, J. J. Qin⁷², L. Q. Qin¹⁴, L. Y. Qin^{71,58}, X. S. Qin⁵⁰, Z. H. Qin^{1,58}, J. F. Qiu¹, Z. H. Qu⁷², C. F. Redmer³⁵, K. J. Ren³⁹, A. Rivetti^{74C}, M. Roloff^{74C}, G. Rong^{1,63}, Ch. Rosner¹⁸, S. N. Ruan⁴³, N. Salone⁴⁴, A. Sarantsev^{36,d}, Y. Schelhaas³⁵, K. Schoenning⁷⁵, M. Scodeggio^{29A}, K. Y. Shan^{12,g}, W. Shan²⁴, X. Y. Shan^{71,58}, Z. J. Shang^{38,k,l}, J. F. Shangguan¹⁶, L. G. Shao^{1,63}, M. Shao^{71,58}, C. P. Shen^{12,g}, H. F. Shen^{1,8}, W. H. Shen⁶³, X. Y. Shen^{1,63}, B. A. Shi⁶³, H. Shi^{71,58}, H. C. Shi^{71,58},

J. L. Shi^{12,g}, J. Y. Shi¹, Q. Q. Shi⁵⁵, S. Y. Shi⁷², X. Shi^{1,58}, J. J. Song¹⁹, T. Z. Song⁵⁹, W. M. Song^{34,1}, Y. J. Song^{12,g}, Y. X. Song^{46,h,n}, S. Sosio^{74A,74C}, S. Spataro^{74A,74C}, F. Stieler³⁵, Y. J. Su⁶³, G. B. Sun⁷⁶, G. X. Sun¹, H. Sun⁶³, H. K. Sun¹, J. F. Sun¹⁹, K. Sun⁶¹, L. Sun⁷⁶, S. S. Sun^{1,63}, T. Sun^{51,f}, W. Y. Sun³⁴, Y. Sun⁹, Y. J. Sun^{71,58}, Y. Z. Sun¹, Z. Q. Sun^{1,63}, Z. T. Sun⁵⁰, C. J. Tang⁵⁴, G. Y. Tang¹, J. Tang⁵⁹, M. Tang^{71,58}, Y. A. Tang⁷⁶, L. Y. Tao⁷², Q. T. Tao^{25,i}, M. Tat⁶⁹, J. X. Teng^{71,58}, V. Thoren⁷⁵, W. H. Tian⁵⁹, Y. Tian^{31,63}, Z. F. Tian⁷⁶, I. Uman^{62B}, Y. Wan⁵⁵, S. J. Wang⁵⁰, B. Wang¹, B. L. Wang⁶³, Bo Wang^{71,58}, D. Y. Wang^{46,h}, F. Wang⁷², H. J. Wang^{38,k,l}, J. J. Wang⁷⁶, J. P. Wang⁵⁰, K. Wang^{1,58}, L. L. Wang¹, M. Wang⁵⁰, N. Y. Wang⁶³, S. Wang^{12,g}, S. Wang^{38,k,l}, T. Wang^{12,g}, T. J. Wang⁴³, W. Wang⁷², W. Wang⁵⁹, W. P. Wang^{35,71,o}, X. Wang^{46,h}, X. F. Wang^{38,k,l}, X. J. Wang³⁹, X. L. Wang^{12,g}, X. N. Wang¹, Y. Wang⁶¹, Y. D. Wang⁴⁵, Y. F. Wang^{1,58,63}, Y. L. Wang¹⁹, Y. N. Wang⁴⁵, Y. Q. Wang¹, Yaqian Wang¹⁷, Yi Wang⁶¹, Z. Wang^{1,58}, Z. L. Wang⁷², Z. Y. Wang^{1,63}, Ziyi Wang⁶³, D. H. Wei¹⁴, F. Weidner⁶⁸, S. P. Wen¹, Y. R. Wen³⁹, U. Wiedner³, G. Wilkinson⁶⁹, M. Wolke⁷⁵, L. Wollenberg³, C. Wu³⁹, J. F. Wu^{1,8}, L. H. Wu¹, L. J. Wu^{1,63}, X. Wu^{12,g}, X. H. Wu³⁴, Y. Wu^{71,58}, Y. H. Wu⁵⁵, Y. J. Wu³¹, Z. Wu^{1,58}, L. Xia^{71,58}, X. M. Xian³⁹, B. H. Xiang^{1,63}, T. Xiang^{46,h}, D. Xiao^{38,k,l}, G. Y. Xiao⁴², S. Y. Xiao¹, Y. L. Xiao^{12,g}, Z. J. Xiao⁴¹, C. Xie⁴², X. H. Xie^{46,h}, Y. Xie⁵⁰, Y. G. Xie^{1,58}, Y. H. Xie⁶, Z. P. Xie^{71,58}, T. Y. Xing^{1,63}, C. F. Xu^{1,63}, C. J. Xu⁵⁹, G. F. Xu¹, H. Y. Xu^{66,2,p}, M. Xu^{71,58}, Q. J. Xu¹⁶, Q. N. Xu³⁰, W. Xu¹, W. L. Xu⁶⁶, X. P. Xu⁵⁵, Y. C. Xu⁷⁷, Z. P. Xu⁴², Z. S. Xu⁶³, F. Yan^{12,g}, L. Yan^{12,g}, W. B. Yan^{71,58}, W. C. Yan⁸⁰, X. Q. Yan¹, H. J. Yang^{51,f}, H. L. Yang³⁴, H. X. Yang¹, T. Yang¹, Y. Yang^{12,g}, Y. F. Yang⁴³, Y. F. Yang^{1,63}, Y. X. Yang^{1,63}, Z. W. Yang^{38,k,l}, Z. P. Yao⁵⁰, M. Ye^{1,58}, M. H. Ye⁸, J. H. Yin¹, Z. Y. You⁵⁹, B. X. Yu^{1,58,63}, C. X. Yu⁴³, G. Yu^{1,63}, J. S. Yu^{25,i}, T. Yu⁷², X. D. Yu^{46,h}, Y. C. Yu⁸⁰, C. Z. Yuan^{1,63}, J. Yuan⁴⁵, J. Yuan³⁴, L. Yuan², S. C. Yuan^{1,63}, Y. Yuan^{1,63}, Z. Y. Yuan⁵⁹, C. X. Yue³⁹, A. A. Zafar⁷³, F. R. Zeng⁵⁰, S. H. Zeng⁷², X. Zeng^{12,g}, Y. Zeng^{25,i}, Y. J. Zeng^{1,63}, Y. J. Zeng⁵⁹, X. Y. Zhai³⁴, Y. C. Zhai⁵⁰, Y. H. Zhan⁵⁹, A. Q. Zhang^{1,63}, B. L. Zhang^{1,63}, B. X. Zhang¹, D. H. Zhang⁴³, G. Y. Zhang¹⁹, H. Zhang⁸⁰, H. Zhang^{71,58}, H. C. Zhang^{1,58,63}, H. H. Zhang⁵⁹, H. H. Zhang³⁴, H. Q. Zhang^{1,58,63}, H. R. Zhang^{71,58}, H. Y. Zhang^{1,58}, J. Zhang⁸⁰, J. Zhang⁵⁹, J. J. Zhang⁵², J. L. Zhang²⁰, J. Q. Zhang⁴¹, J. S. Zhang^{12,g}, J. W. Zhang^{1,58,63}, J. X. Zhang^{38,k,l}, J. Y. Zhang¹, J. Z. Zhang^{1,63}, Jianyu Zhang⁶³, L. M. Zhang⁶¹, Lei Zhang⁴², P. Zhang^{1,63}, Q. Y. Zhang³⁴, R. Y. Zhang^{38,k,l}, S. H. Zhang^{1,63}, Shulei Zhang^{25,i}, X. D. Zhang⁴⁵, X. M. Zhang¹, X. Y. Zhang⁵⁰, Y. Zhang⁷², Y. Zhang¹, Y. T. Zhang⁸⁰, Y. H. Zhang^{1,58}, Y. M. Zhang³⁹, Yan Zhang^{71,58}, Z. D. Zhang¹, Z. H. Zhang¹, Z. L. Zhang³⁴, Z. Y. Zhang⁴³, Z. Y. Zhang⁷⁶, Z. Z. Zhang⁴⁵, G. Zhao¹, J. Y. Zhao^{1,63}, J. Z. Zhao^{1,58}, L. Zhao¹, Lei Zhao^{71,58}, M. G. Zhao⁴³, N. Zhao⁷⁸, R. P. Zhao⁶³, S. J. Zhao⁸⁰, Y. B. Zhao^{1,58}, Y. X. Zhao^{31,63}, Z. G. Zhao^{71,58}, A. Zhemchugov^{36,b}, B. Zheng⁷², B. M. Zheng³⁴, J. P. Zheng^{1,58}, W. J. Zheng^{1,63}, Y. H. Zheng⁶³, B. Zhong⁴¹, X. Zhong⁵⁹, H. Zhou⁵⁰, J. Y. Zhou³⁴, L. P. Zhou^{1,63}, S. Zhou⁶, X. Zhou⁷⁶, X. K. Zhou⁶, X. R. Zhou^{71,58}, X. Y. Zhou³⁹, Y. Z. Zhou^{12,g}, J. Zhu⁴³, K. Zhu¹, K. J. Zhu^{1,58,63}, K. S. Zhu^{12,g}, L. Zhu³⁴, L. X. Zhu⁶³, S. H. Zhu⁷⁰, S. Q. Zhu⁴², T. J. Zhu^{12,g}, W. D. Zhu⁴¹, Y. C. Zhu^{71,58}, Z. A. Zhu^{1,63}, J. H. Zou¹, J. Zu^{71,58}

(BESIII Collaboration)

¹ Institute of High Energy Physics, Beijing 100049, People's Republic of China

² Beihang University, Beijing 100191, People's Republic of China

³ Bochum Ruhr-University, D-44780 Bochum, Germany

⁴ Budker Institute of Nuclear Physics SB RAS (BINP), Novosibirsk 630090, Russia

⁵ Carnegie Mellon University, Pittsburgh, Pennsylvania 15213, USA

⁶ Central China Normal University, Wuhan 430079, People's Republic of China

⁷ Central South University, Changsha 410083, People's Republic of China

⁸ China Center of Advanced Science and Technology, Beijing 100190, People's Republic of China

⁹ China University of Geosciences, Wuhan 430074, People's Republic of China

¹⁰ Chung-Ang University, Seoul, 06974, Republic of Korea

¹¹ COMSATS University Islamabad, Lahore Campus, Defence Road, Off Raiwind Road, 54000 Lahore, Pakistan

¹² Fudan University, Shanghai 200433, People's Republic of China

¹³ GSI Helmholtzcentre for Heavy Ion Research GmbH, D-64291 Darmstadt, Germany

¹⁴ Guangxi Normal University, Guilin 541004, People's Republic of China

¹⁵ Guangxi University, Nanning 530004, People's Republic of China

¹⁶ Hangzhou Normal University, Hangzhou 310036, People's Republic of China

¹⁷ Hebei University, Baoding 071002, People's Republic of China

- ¹⁸ Helmholtz Institute Mainz, Staudinger Weg 18, D-55099 Mainz, Germany
¹⁹ Henan Normal University, Xinxiang 453007, People's Republic of China
²⁰ Henan University, Kaifeng 475004, People's Republic of China
²¹ Henan University of Science and Technology, Luoyang 471003, People's Republic of China
²² Henan University of Technology, Zhengzhou 450001, People's Republic of China
²³ Huangshan College, Huangshan 245000, People's Republic of China
²⁴ Hunan Normal University, Changsha 410081, People's Republic of China
²⁵ Hunan University, Changsha 410082, People's Republic of China
²⁶ Indian Institute of Technology Madras, Chennai 600036, India
²⁷ Indiana University, Bloomington, Indiana 47405, USA
²⁸ INFN Laboratori Nazionali di Frascati , (A)INFN Laboratori Nazionali di Frascati, I-00044, Frascati, Italy; (B)INFN Sezione di Perugia, I-06100, Perugia, Italy; (C)University of Perugia, I-06100, Perugia, Italy
²⁹ INFN Sezione di Ferrara, (A)INFN Sezione di Ferrara, I-44122, Ferrara, Italy; (B)University of Ferrara, I-44122, Ferrara, Italy
³⁰ Inner Mongolia University, Hohhot 010021, People's Republic of China
³¹ Institute of Modern Physics, Lanzhou 730000, People's Republic of China
³² Institute of Physics and Technology, Peace Avenue 54B, Ulaanbaatar 13330, Mongolia
³³ Instituto de Alta Investigación, Universidad de Tarapacá, Casilla 7D, Arica 1000000, Chile
³⁴ Jilin University, Changchun 130012, People's Republic of China
³⁵ Johannes Gutenberg University of Mainz, Johann-Joachim-Becher-Weg 45, D-55099 Mainz, Germany
³⁶ Joint Institute for Nuclear Research, 141980 Dubna, Moscow region, Russia
³⁷ Justus-Liebig-Universitaet Giessen, II. Physikalisches Institut, Heinrich-Buff-Ring 16, D-35392 Giessen, Germany
³⁸ Lanzhou University, Lanzhou 730000, People's Republic of China
³⁹ Liaoning Normal University, Dalian 116029, People's Republic of China
⁴⁰ Liaoning University, Shenyang 110036, People's Republic of China
⁴¹ Nanjing Normal University, Nanjing 210023, People's Republic of China
⁴² Nanjing University, Nanjing 210093, People's Republic of China
⁴³ Nankai University, Tianjin 300071, People's Republic of China
⁴⁴ National Centre for Nuclear Research, Warsaw 02-093, Poland
⁴⁵ North China Electric Power University, Beijing 102206, People's Republic of China
⁴⁶ Peking University, Beijing 100871, People's Republic of China
⁴⁷ Qufu Normal University, Qufu 273165, People's Republic of China
⁴⁸ Renmin University of China, Beijing 100872, People's Republic of China
⁴⁹ Shandong Normal University, Jinan 250014, People's Republic of China
⁵⁰ Shandong University, Jinan 250100, People's Republic of China
⁵¹ Shanghai Jiao Tong University, Shanghai 200240, People's Republic of China
⁵² Shanxi Normal University, Linfen 041004, People's Republic of China
⁵³ Shanxi University, Taiyuan 030006, People's Republic of China
⁵⁴ Sichuan University, Chengdu 610064, People's Republic of China
⁵⁵ Soochow University, Suzhou 215006, People's Republic of China
⁵⁶ South China Normal University, Guangzhou 510006, People's Republic of China
⁵⁷ Southeast University, Nanjing 211100, People's Republic of China
⁵⁸ State Key Laboratory of Particle Detection and Electronics, Beijing 100049, Hefei 230026, People's Republic of China
⁵⁹ Sun Yat-Sen University, Guangzhou 510275, People's Republic of China
⁶⁰ Suranaree University of Technology, University Avenue 111, Nakhon Ratchasima 30000, Thailand
⁶¹ Tsinghua University, Beijing 100084, People's Republic of China
⁶² Turkish Accelerator Center Particle Factory Group, (A)Istinye University, 34010, Istanbul, Turkey; (B)Near East University, Nicosia, North Cyprus, 99138, Mersin 10, Turkey
⁶³ University of Chinese Academy of Sciences, Beijing 100049, People's Republic of China
⁶⁴ University of Groningen, NL-9747 AA Groningen, The Netherlands

- ⁶⁵ University of Hawaii, Honolulu, Hawaii 96822, USA
⁶⁶ University of Jinan, Jinan 250022, People's Republic of China
⁶⁷ University of Manchester, Oxford Road, Manchester, M13 9PL, United Kingdom
⁶⁸ University of Muenster, Wilhelm-Klemm-Strasse 9, 48149 Muenster, Germany
⁶⁹ University of Oxford, Keble Road, Oxford OX13RH, United Kingdom
⁷⁰ University of Science and Technology Liaoning, Anshan 114051, People's Republic of China
⁷¹ University of Science and Technology of China, Hefei 230026, People's Republic of China
⁷² University of South China, Hengyang 421001, People's Republic of China
⁷³ University of the Punjab, Lahore-54590, Pakistan
⁷⁴ University of Turin and INFN, (A)University of Turin, I-10125, Turin, Italy; (B)University of Eastern Piedmont, I-15121, Alessandria, Italy; (C)INFN, I-10125, Turin, Italy
⁷⁵ Uppsala University, Box 516, SE-75120 Uppsala, Sweden
⁷⁶ Wuhan University, Wuhan 430072, People's Republic of China
⁷⁷ Yantai University, Yantai 264005, People's Republic of China
⁷⁸ Yunnan University, Kunming 650500, People's Republic of China
⁷⁹ Zhejiang University, Hangzhou 310027, People's Republic of China
⁸⁰ Zhengzhou University, Zhengzhou 450001, People's Republic of China
- ^a Deceased
- ^b Also at the Moscow Institute of Physics and Technology, Moscow 141700, Russia
^c Also at the Novosibirsk State University, Novosibirsk, 630090, Russia
^d Also at the NRC "Kurchatov Institute", PNPI, 188300, Gatchina, Russia
^e Also at Goethe University Frankfurt, 60323 Frankfurt am Main, Germany
^f Also at Key Laboratory for Particle Physics, Astrophysics and Cosmology, Ministry of Education; Shanghai Key Laboratory for Particle Physics and Cosmology; Institute of Nuclear and Particle Physics, Shanghai 200240, People's Republic of China
^g Also at Key Laboratory of Nuclear Physics and Ion-beam Application (MOE) and Institute of Modern Physics, Fudan University, Shanghai 200443, People's Republic of China
^h Also at State Key Laboratory of Nuclear Physics and Technology, Peking University, Beijing 100871, People's Republic of China
ⁱ Also at School of Physics and Electronics, Hunan University, Changsha 410082, China
^j Also at Guangdong Provincial Key Laboratory of Nuclear Science, Institute of Quantum Matter, South China Normal University, Guangzhou 510006, China
^k Also at MOE Frontiers Science Center for Rare Isotopes, Lanzhou University, Lanzhou 730000, People's Republic of China
^l Also at Lanzhou Center for Theoretical Physics, Lanzhou University, Lanzhou 730000, People's Republic of China
^m Also at the Department of Mathematical Sciences, IBA, Karachi 75270, Pakistan
ⁿ Also at Ecole Polytechnique Federale de Lausanne (EPFL), CH-1015 Lausanne, Switzerland
^o Also at Helmholtz Institute Mainz, Staudinger Weg 18, D-55099 Mainz, Germany
^p Also at School of Physics, Beihang University, Beijing 100191 , China

Based on 6.1 fb^{-1} of e^+e^- annihilation data collected at center-of-mass energies from 4.600 to 4.843 GeV with the BESIII detector at the BEPCII collider, a partial wave analysis of $\Lambda_c^+ \rightarrow \Lambda\pi^+\eta$ is performed, and branching fractions and decay asymmetry parameters of intermediate processes are determined. The process $\Lambda_c^+ \rightarrow \Lambda a_0(980)^+$ is observed for the first time, and evidence for the pentaquark candidate $\Sigma(1380)^+$ decaying into $\Lambda\pi^+$ is found with statistical significance larger than 3σ with mass and width fixed to theoretical predictions. The branching fraction product $\mathcal{B}[\Lambda_c^+ \rightarrow \Lambda a_0(980)^+] \mathcal{B}[a_0(980)^+ \rightarrow \pi^+\eta]$ is determined to be $(1.05 \pm 0.16_{\text{stat}} \pm 0.05_{\text{syst}} \pm 0.07_{\text{ext}})\%$, which is larger than theoretical calculations by 1-2 orders of magnitude. Here the third (external) systematic is from $\mathcal{B}(\Lambda_c^+ \rightarrow \Lambda\pi^+\eta)$. Finally, we precisely obtain the absolute branching fraction $\mathcal{B}(\Lambda_c^+ \rightarrow \Lambda\pi^+\eta) = (1.94 \pm 0.07_{\text{stat}} \pm 0.11_{\text{syst}})\%$.

Apart from the traditional bound states like mesons and baryons, the quark model [1, 2] allows for more

complex structures such as tetraquarks, pentaquarks, hybrids, glueballs, and hadronic molecular states. For the

studies of these exotic states, many important achievements have been made [3–9], especially in quarkonium, D meson, and B meson decays. Studies of baryon decays are relatively rare, except for studies of Λ_b^0 decays into P_c or $X(3872)$ states by the LHCb experiment [10–12]. Replacing the b quark with a c quark, the much lighter charm baryons lie at the boundary between perturbative and nonperturbative regions. Given the very interesting results already achieved in the first studies of heavy exotic states in bottom baryon decays, studies using charm baryon decays provide a new and exciting opportunity to probe lighter exotic states.

The exact nature of the scalar meson $a_0(980)^+$ remains elusive, with various interpretations proposed. These include a conventional $q\bar{q}$ meson [13, 14], a compact tetraquark [15, 16], a superposition of both [17], or a dynamically generated threshold effect [18–22]. Reference [23] adopted the compact tetraquark assumption to study the $\Lambda_c^+ \rightarrow \Lambda a_0(980)^+$ decay, as the $q\bar{q}$ picture failed to explain the measured $\mathcal{B}[\Lambda_c^+ \rightarrow p f_0(980)]$ [24], where the $f_0(980)$ is regarded as the scalar octet partner of $a_0(980)^+$ in the $q\bar{q}$ model. The $\Lambda_c^+ \rightarrow \Lambda a_0(980)^+$ branching fraction (BF) was calculated to be 1.9×10^{-4} based on factorization and the pole model, where the pole term was found to dominate over factorizable contributions. In a different perspective, Ref. [25] proposed a significant enhancement of the BF to $(1.7^{+2.8}_{-1.0} \pm 0.3) \times 10^{-3}$ by considering the process $\Lambda_c^+ \rightarrow \Sigma(1385)^+\eta$, followed by rescattering $\Sigma(1385)^+\eta \rightarrow \Lambda a_0(980)^+$. Here, the calculated $\mathcal{B}[\Lambda_c^+ \rightarrow \Sigma(1385)^+\eta]$ in the topological scheme [26] is employed as an input. Contributions from other processes, such as $\Lambda_c^+ \rightarrow \Lambda(1670)\pi^+ \rightarrow \Lambda a_0(980)^+$ and the triangle singularity enhanced $\Lambda_c^+ \rightarrow \Sigma^*\eta(N^*\bar{K}^0) \rightarrow \Lambda a_0(980)^+$, are estimated to be less than 1×10^{-3} . Moreover, due to the proximity of the $a_0(980)^+$ pole mass to the $K\bar{K}$ threshold, the $a_0(980)^+$ line shape exhibits a distinct cusp structure, a characteristic feature indicative of its molecular nature [27]. Therefore, the $\Lambda_c^+ \rightarrow \Lambda\pi^+\eta$ decay provides a good platform to study the internal structure of $a_0(980)^+$.

The study of low-lying excited baryons with $J^P = 1/2^-$ is crucial in hadron physics [28]. Historically, to address the reverse mass-order reverse of the $N(1535)$ and $\Lambda(1405)$ states, theorists proposed the pentaquark model [29–31] and the meson cloud and molecular model [32, 33]. These models predict the lowest $\Sigma_{1/2-}^*$ resonance around 1380 MeV/ c^2 [34], close to the $N\bar{K}$ mass threshold [35]. Experimental and theoretical investigations on $\Sigma(1380)^+$ as well as other light pentaquark states containing strange quarks have been conducted in various processes [31, 34, 36–57]. However, establishing the lowest $\Sigma_{1/2-}^*$ resonance remains a challenge. The $\Lambda_c^+ \rightarrow \Lambda\pi^+\eta$ decay has been highlighted as a golden channel [58, 59]. The $\Lambda\pi^+$ mode, representing a pure

$I = 1$ combination, excludes influences from Λ^* resonances as compared to the $\Sigma\pi$ and pK modes. Also, the influences from the $\Sigma(1385)^+$ and $\Lambda(1670)$ [60, 61] on the $\Sigma(1380)^+$ can be distinguished. This is because $\Lambda(1670)$ predominantly affects the high end of the $M(\Lambda\pi^+)$ spectrum, while the $\Sigma(1385)^+$ exhibits a different spin-parity resulting in a distinct angular distribution.

In this Letter, the first partial wave analysis (PWA) of the $\Lambda_c^+ \rightarrow \Lambda\pi^+\eta$ decay is performed by using 11 datasets at center-of-mass (c.m.) energies from 4.600 to 4.843 GeV [62–66], where Λ_c^+ is dominantly produced via pair production $e^+e^- \rightarrow \Lambda_c^+\bar{\Lambda}_c^-$. There is no sufficient energy for producing additional hadrons below 4.7 GeV, and the process $e^+e^- \rightarrow \Lambda_c^+\bar{\Lambda}_c^-\pi^0$ is highly suppressed between 4.7 and 4.843 GeV. The datasets used are accumulated with the BESIII detector at the BEPCII collider and correspond to an integrated luminosity of 6.1 fb^{-1} . Detailed information about BESIII and BEPCII can be found in Refs. [67–70]. The simulated “inclusive Monte Carlo (MC) sample” is described in Ref. [72]. In the “phase-space (PHSP) signal MC sample” and the “PWA signal MC sample”, $\Lambda_c^+ \rightarrow \Lambda\pi^+\eta$ decays are simulated with a uniform PHSP distribution and our PWA result, respectively, while the $\bar{\Lambda}_c^-$ decays inclusively. Throughout this Letter, charge-conjugate modes are implied unless explicitly noted.

We use a single-tag (ST) method [71], where the Λ_c^+ is reconstructed via the cascade decays $\Lambda_c^+ \rightarrow \Lambda\pi^+\eta$, $\Lambda \rightarrow p\pi^-$, $\eta \rightarrow \gamma\gamma$ and $\eta \rightarrow \pi^+\pi^-\pi^0$, $\pi^0 \rightarrow \gamma\gamma$. The requirements for selecting charged tracks, photon showers, and particle identification (PID) for the proton and pion follow the previous BESIII analysis [72]. To reconstruct Λ candidates, the $p\pi^-$ pairs are constrained to originate from a common vertex by requiring the χ^2 of a vertex fit to be less than 100 and the $p\pi^-$ invariant mass to satisfy $1.08 < M_{p\pi^-} < 1.15 \text{ GeV}/c^2$. To reconstruct $\eta, \pi^0 \rightarrow \gamma\gamma$ candidates, the $\gamma\gamma$ invariant mass $M_{\gamma\gamma}$ is required to be within $[0.500, 0.600] \text{ GeV}/c^2$ ($[0.105, 0.150] \text{ GeV}/c^2$). To improve the momentum resolution, a one-constraint kinematic fit is performed by constraining $M_{\gamma\gamma}$ to the known η, π^0 masses [73], and the fit χ^2 must be less than 20 (200). The updated momenta are used in further analysis. To reconstruct $\eta \rightarrow \pi^+\pi^-\pi^0$ candidates, the $\pi^+\pi^-\pi^0$ invariant mass, $M_{\pi^+\pi^-\pi^0}$, is required to be within $(0.500, 0.600) \text{ GeV}/c^2$. If there are multiple Λ_c^+ combinations in an event, we choose the candidate with the minimum magnitude of the energy difference, defined as $\Delta E \equiv E_{\Lambda_c} - E_{\text{beam}}$, where E_{Λ_c} is the energy of the detected Λ_c^+ candidate in the e^+e^- rest frame, and E_{beam} is the beam energy. Furthermore, the requirement $-0.1 < \Delta E < 0.1 \text{ GeV}$ is imposed.

To further suppress the backgrounds, a boosted decision tree with gradient boosting (BDTG) [74] based on the TMVA package [75] is used. The input variables are ΔE , $M_{p\pi^-}$, the ratio of the Λ decay length to its uncertainty L/σ_L , $M_{\gamma\gamma}$, $M_{\pi^+\pi^-\pi^0}$

(only for $\eta \rightarrow \pi^+ \pi^- \pi^0$ channel), the cosine of the helicity angle of $\eta, \pi^0 \rightarrow \gamma\gamma$ decay, $\cos \theta_{\eta(\pi^0)}$, and the lateral moments of the showers with higher and lower energies $\text{Lat}(\gamma_{\text{High}})$ and $\text{Lat}(\gamma_{\text{Low}})$. The inclusive MC sample is input as the training set, in which the signal and nonsignal processes are tagged as signal and background, respectively. The resultant BDTG scores are required to be greater than 0.95 and 0.97 for the $\eta \rightarrow \gamma\gamma$ and $\eta \rightarrow \pi^+ \pi^- \pi^0$ channels, respectively, chosen by optimizing the figure-of-merit $\text{FOM} = \frac{S}{\sqrt{S+B}} \frac{S}{S+B}$. Here, S (B) is the number of signal (background) events in the inclusive MC sample whose luminosity is normalized to the data.

An extended unbinned maximum likelihood fit is performed on the beam-constrained mass, $M_{\text{BC}} = \sqrt{E_{\text{beam}}^2 - |\vec{p}|^2}$, distribution [71] of each energy point to obtain the signal yields and purity in data, where \vec{p} is the three-momentum of the ST Λ_c^+ candidate and E_{beam} is the beam energy, both evaluated in the e^+e^- center-of-mass system. The method is the same as Ref. [72], and 1312 ± 45 signal events are obtained with purity of about 80% in the signal regions, as shown in Supplemental Material [76]. The result of the fit to the M_{BC} distribution from the combined $\eta \rightarrow \gamma\gamma$ and $\eta \rightarrow \pi^+ \pi^- \pi^0$ channels at 4.682 GeV is shown in Fig. 1, and the results at other energy points are shown in Supplemental Material [76]. The event-by-event sWeight factor is calculated by the sPlot method [81], according to the fit results. The sPlot method is a statistical tool dedicated to the exploration of data samples populated by several sources of events, e.g., signal and background. The sWeight factor as a function of discriminating variable like M_{BC} is designed such that it is normal to signal distribution but orthogonal to background distribution. After applying the sWeight factor, background does not contribute to the extracted signal distribution. In order to improve the momentum resolution, an additional three-constraint kinematic fit is applied, in which the $\Lambda\pi^+\eta$ invariant mass and the recoiled $\bar{\Lambda}_c^-$ mass are constrained to the known Λ_c^+ mass, and the $p\pi^-$ invariant mass is constrained to the known Λ mass [73]. The recoiled $\bar{\Lambda}_c^-$ momentum is calculated with the momentum of the initial e^+e^- system and $\Lambda\pi^+\eta$ momentum. The updated momenta of the signal candidates from the kinematic fit are used in the PWA.

In the framework of the helicity amplitude formalism [82, 83], a PWA is performed by using the open-source framework TF-PWA [84]. The fundamental concepts follow Ref. [72]. In this Letter, the amplitude is defined in the e^+e^- rest frame. The parameters describing the amplitude of the $\Lambda_c^+ \rightarrow \Lambda\pi^+\eta$ decay are shared for each energy point. Moreover, the parameters describing the amplitude of the $\bar{\Lambda}_c^-$ decay are related to those of Λ_c^+ via a parity transformation on the $\bar{\Lambda}_c^-$ candidates, under the assumption of CP conservation. The Λ_c^+ polarization components are fixed to $P_z = P_x = 0$, $P_y(\theta_{ee}, \alpha_0, \Delta_0) \propto$

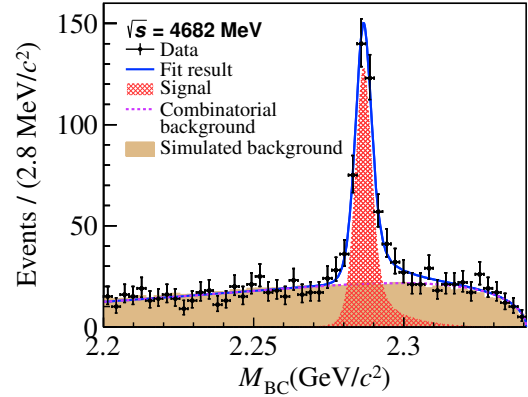


FIG. 1. The fit to the M_{BC} distribution combined from the $\eta \rightarrow \gamma\gamma$ and $\eta \rightarrow \pi^+ \pi^- \pi^0$ channels at 4.682 GeV. The points with error bars are data, the brown solid histogram is MC-simulated background, the red hatched histogram is signal, the violet dashed line is background shape, and the blue line is total fit.

$\sqrt{1 - \alpha_0^2} \sin \theta_{ee} \cos \theta_{ee} \sin \Delta_0$ [85]. Here, θ_{ee} is the polar angle of the Λ_c^+ with respect to the e^+ beam in the e^+e^- c.m. system, α_0 is fixed to the values from Refs. [86, 87], and Δ_0 is fixed according to polarization results in data. The decay amplitudes of the Λ_c^+ decay are described with sequential helicity amplitudes for cascade quasi-two-body decay and the propagators of intermediate states. For decay chains with resonant intermediate states, the barrier factor term is included. For those with nonresonant (NR) intermediate states, the barrier factor term is omitted.

In the decay amplitude of $\Lambda_c^+ \rightarrow \Lambda a_0(980)^+$, $a_0(980)^+ \rightarrow \pi^+ \eta$, the propagator of the $a_0(980)^+$ is described by the two coupled-channel Flatté model [88]. The nominal mass and coupling constants of the $a_0(980)^+$ decaying to the $\eta\pi$ and $K\bar{K}$ coupled channels are quoted from Ref. [89]. For the NR decay, the dynamical function is set to be unity. In the decay chains of $\Lambda_c^+ \rightarrow \Sigma(1385)^+ \eta$, $\Sigma(1385)^+ \rightarrow \Lambda\pi^+$ and $\Lambda_c^+ \rightarrow \Lambda(1670)\pi^+$, $\Lambda(1670) \rightarrow \Lambda\eta$, the relativistic Breit-Wigner (RBW) formula [72] is used as the propagator of the $\Sigma(1385)^+$ and $\Lambda(1670)$. The nominal mass and width of the $\Sigma(1385)^+$ are fixed to the corresponding values from the Particle Data Group (PDG) [73], and those of $\Lambda(1670)$ are taken from a recent measurement [90]. The amplitude of $\Lambda \rightarrow p\pi^-$ is constrained according to the decay asymmetry α_Λ from the PDG [73]. The full amplitude is the coherent sum of amplitudes of all decay chains, and the alignment D functions are considered to align the helicities of the final state protons [60, 91]. The construction of the signal probability density function and the derivations of fit fractions (FFs), interference, and corresponding statistical uncertainties follow the previous BESIII analysis [72]. The negative log-likelihood (NLL) is a sum over of all signal

candidates considering the sWeight factor w_i of i th event, $-\ln L = -a \sum_{i \in \text{data}} w_i \ln P(p_i)$ with the normalization factor $a = \sum_{i \in \text{data}} w_i / \sum_{i \in \text{data}} w_i^2$ [92].

To determine the baseline solution of PWA, significant resonances $\Sigma(1385)^+$, $\Lambda(1670)$, and $a_0(980)^+$ are added in the first trial. In the second iteration, other possible components are added one by one. The \mathcal{S} wave $\pi^+ \eta$ NR component NR_{0+} with highest significance is chosen. In the third iteration, the statistical significances of these amplitudes are all greater than 5σ , as shown in Table I, and no other resonant component exceeds this threshold. The statistical significance is calculated from the change of the NLL values with and without including the component, taking into account the change of the number of degrees of freedom (d.o.f.). The fit results projected on different mass spectra are shown in Fig. 2. The fit results for the FFs and decay asymmetry parameters are listed in Table I, where the decay asymmetry parameter arises from the interference between partial wave amplitudes. Using fits to samples from pseudo-experiments, each matched to the data statistics, the pull distribution of each parameter is obtained. We correct the central value and scale the statistical uncertainty for a parameter if its pull distribution deviates significantly from the normal distribution. Since the fitted $\alpha_{\Lambda a_0(980)^+}$ value is very close to its physical limit, an asymmetric statistical uncertainty is derived by scanning the NLL.

TABLE I. Fit fractions, statistical significances \mathcal{S} , and decay asymmetry parameters α for different components in the baseline solution. The total FF is 113.9%. The first uncertainty is statistical, and the second is systematic.

Process	FF (%)	\mathcal{S}	α
$\Lambda a_0(980)^+$	$54.0 \pm 8.4 \pm 2.6$	13.1σ	$-0.91^{+0.18}_{-0.09} \pm 0.08$
$\Sigma(1385)^+ \eta$	$30.4 \pm 2.6 \pm 0.7$	22.5σ	$-0.61 \pm 0.15 \pm 0.04$
$\Lambda(1670) \pi^+$	$14.1 \pm 2.8 \pm 1.2$	11.7σ	$0.21 \pm 0.27 \pm 0.33$
ANR_{0+}	15.4 ± 5.3	6.7σ	...

Adopting the Breit-Wigner mass and width values of 1380 MeV/ c^2 and 120 MeV, respectively, as predicted in Refs. [34, 58], the potential pentaquark state $\Sigma(1380)^+$ is investigated in the signal process. In the construction of the baseline solution, NR_{0+} is introduced to better describe data with statistical significance of 6.7σ , while that of the $\Sigma(1380)^+$ is slightly lower. To investigate the statistical significance of $\Sigma(1380)^+$, we construct ‘‘model A’’ [$\Lambda a_0(980)^+$, $\Sigma(1385)^+ \eta$, $\Lambda(1670) \pi^+$, $\Sigma(1380)^+ \eta$] and ‘‘model B’’ [$\Lambda a_0(980)^+$, $\Sigma(1385)^+ \eta$, $\Lambda(1670) \pi^+$, $\Sigma(1380)^+ \eta$, ANR_{0+}]. Comparing model A (model B) with and without $\Sigma(1380)^+$, the statistical significance is determined to be 6.1σ (3.3σ) under model assumption of mass and width fixed to Refs. [34, 58]. The change in NLL is 24.1 and 9.2 for model A and model B, respectively, while number of d.o.f. changes are both 4. Projections onto the $M_{\Lambda \pi^+}$ spectrum for models A and B are illus-

trated in Fig. 3 left and middle, while the corresponding results for the FFs are detailed in Table II. Despite the overall significance of NR_{0+} being higher than that of $\Sigma(1380)^+$, a subtle preference for $\Sigma(1380)^+$ over NR_{0+} is discerned from the Σ^+ helicity angle distribution in the $a_0(980)^+$ signal region, $M_{\Lambda \pi^+} > 1.44 \text{ GeV}/c^2$ and $M_{\Lambda \eta} > 1.72 \text{ GeV}/c^2$. The comparison plot is shown in Fig. 3 right, and more details can be found in Supplemental Material [76]. Additionally, various models are tested by replacing NR_{0+} with other excited states such as Σ^{*+} , Λ^* , a_0^+ , and a_2^+ , while considering systematic uncertainties arising from fixed mass and width parameters by varying them within $\pm 1\sigma$ [34], or float mass and width parameters. In all cases, the calculated statistical significances exceed 3σ . Consequently, this study presents the first evidence for the $\Sigma(1380)^+$.

TABLE II. Fit results of FFs and statistical significances for different components in alternative models including $\Sigma(1380)^+$. The total FFs are 115.8% and 119.8% for models A and B, respectively. The uncertainties are statistical only.

Process	Model A	Model B
$\Lambda a_0(980)^+$	$52.9 \pm 4.5 (13.4\sigma)$	$50.6 \pm 8.0 (11.1\sigma)$
$\Sigma(1385)^+ \eta$	$36.6 \pm 2.6 (15.8\sigma)$	$31.3 \pm 3.0 (14.6\sigma)$
$\Lambda(1670) \pi^+$	$10.7 \pm 1.4 (15.0\sigma)$	$9.0 \pm 1.6 (11.9\sigma)$
$\Sigma(1380)^+ \eta$	$15.5 \pm 4.4 (6.1\sigma)$	$17.7 \pm 5.7 (3.3\sigma)$
ANR_{0+}	...	$11.3 \pm 4.4 (4.2\sigma)$

The line shapes of the $a_0(980)^+$ and $\Lambda(1670)$ are also tested with the Final-State-Interaction (FSI) model [27], and alternative PWA fits are performed. No significant differences are observed in the results of the RBW and FSI models, but the interference between $a_0(980)^+$ and NR_{0+} is very large if the Flatté model is replaced by the FSI model. However, if we remove NR_{0+} and refit the data, there is an obvious discrepancy between data and fit. Details can be found in Supplemental Material [76].

In the measurement of the absolute BF of $\Lambda_c^+ \rightarrow \Lambda \pi^+ \eta$, the selection criteria are almost the same as those used to select the PWA sample except for the requirements of BDTG scores. The requirements of BDTG scores are optimized to be greater than 0.93 and 0.94 for the $\eta \rightarrow \gamma\gamma$ and $\eta \rightarrow \pi^+ \pi^- \pi^0$ channels, respectively, by using an alternative FOM, $S/\sqrt{S+B}$. Extended unbinned maximum likelihood fits are performed to the M_{BC} distribution, simultaneously at each energy point. In the fit, four components are considered, including signal, mismatched background, Λ_c^+ decay backgrounds which are derived from MC simulation, and combinatorial background modeled with an ARGUS function [93]. A truth-match method [94] is employed to separate signals and mismatched backgrounds. The yield ratios of signals and mismatched backgrounds and Λ_c^+ decay backgrounds are

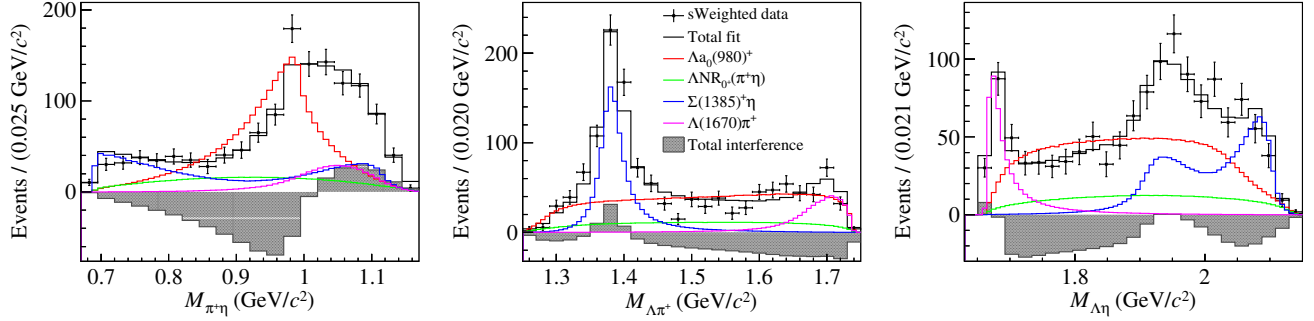


FIG. 2. Projections of the fit results in the $M_{\pi^+\eta}$, $M_{\Lambda\pi^+}$, and $M_{\Lambda\eta}$ spectra. Points with error bars are sWeighted data at all energy points. The curves in different colors are different components.

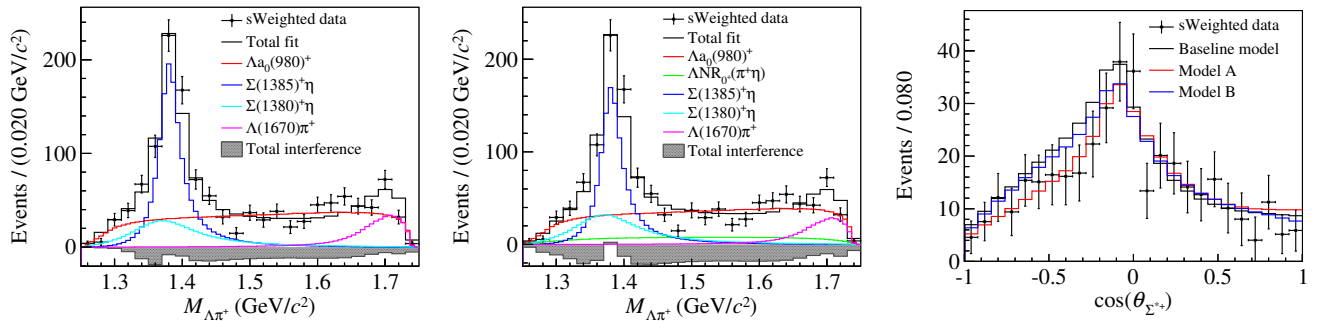


FIG. 3. Left/middle: projections of models A and B on the $M_{\Lambda\pi^+}$ spectrum, respectively, where points with error bars are sWeighted data, and the curves in different colors are different components. Right: projections of the baseline model, models A and B on the Σ^{*+} helicity angle, $\cos \theta_{\Sigma^{*+}}$, with the curve indicating the total fit.

fixed according to MC simulation. The total signal yield is given by $N_{\text{sig}} = 2 \times N_{\Lambda_c^+ \bar{\Lambda}_c^-} \times \mathcal{B} \times \mathcal{B}_{\text{inter}} \times \varepsilon$. Here, $N_{\Lambda_c^+ \bar{\Lambda}_c^-}$ is the number of $\Lambda_c^+ \bar{\Lambda}_c^-$ pairs calculated from the luminosities and cross sections [64, 65, 86, 87], and \mathcal{B} is the BF of the signal decay shared for all c.m. energy points, $\mathcal{B}_{\text{inter}} = \mathcal{B}(\Lambda \rightarrow p\pi^-) \cdot \mathcal{B}(\eta \rightarrow \gamma\gamma)$ and $\mathcal{B}(\Lambda \rightarrow p\pi^-) \cdot \mathcal{B}(\eta \rightarrow \pi^+\pi^-\pi^0) \cdot \mathcal{B}(\pi^0 \rightarrow \gamma\gamma)$ is the BF of intermediate decays quoted from the PDG [73]. Finally, ε is the average detection efficiency based on PWA signal MC samples in which Λ_c^+ decays follow decay amplitudes with parameters fixed by PWA results: $(13.73 \pm 0.02)\%$ and $(4.83 \pm 0.01)\%$ for the $\eta \rightarrow \gamma\gamma$, and $\eta \rightarrow \pi^+\pi^-\pi^0$ channels, respectively. The uncertainties are statistical only. The BF is determined to be $(1.94 \pm 0.07)\%$ which is consistent with the previous measurements [60, 61, 73]. The fit plots can be found in Supplemental Material [76].

The systematic uncertainties on the measurement of the FFs and decay asymmetry parameters include the fixed parameters, barrier radius, additional resonant components, Λ_c^+ polarization, fit method, differences between data and MC simulation, and background descriptions. The total systematic uncertainty on the BF measurement is evaluated to be 5.7% including tracking (0.9%), PID (0.3%), Λ reconstruction (2.6%), η reconstruction (1.0%), BDTG score requirements (1.1%), signal model (2.7%), fit model (0.9%), $\mathcal{B}_{\text{inter}}$ (0.9%), $N_{\Lambda_c^+ \bar{\Lambda}_c^-}$

(3.9%), and MC statistics (0.4%). Details for both the PWA and BF results can be found in Supplemental Material [76].

In summary, based on 6.1 fb^{-1} of e^+e^- annihilation data collected at the c.m. energy region between 4.600 and 4.843 GeV with the BESIII detector, the first PWA of $\Lambda_c^+ \rightarrow \Lambda\pi^+\eta$ is performed. The $\Lambda_c^+ \rightarrow \Lambda a_0(980)^+$ decay is observed for the first time, with a statistical significance of 13.1σ , and evidence for the potential pentaquark state $\Sigma(1380)^+$ is found in the $\Lambda\pi^+$ system via a PWA, with a statistical significance larger than 3σ . The BF of $\Lambda_c^+ \rightarrow \Lambda\pi^+\eta$ is measured to be $(1.94 \pm 0.07_{\text{stat}} \pm 0.01_{\text{syst}})\%$, which is consistent with the previous results of BESIII [60] and Belle [61]. The product BF of $\Lambda_c^+ \rightarrow \Lambda a_0(980)^+$ and $a_0(980)^+ \rightarrow \pi^+\eta$ is calculated to be $(1.05 \pm 0.16 \pm 0.05 \pm 0.07)\%$, where the first and second uncertainties are quoted from those of FF value, while the third is due to $\mathcal{B}(\Lambda_c^+ \rightarrow \Lambda\pi^+\eta)$. Taking $\mathcal{B}[a_0(980)^+ \rightarrow \pi^+\eta] = 0.853 \pm 0.014$ [95], the BF of $\Lambda_c^+ \rightarrow \Lambda a_0(980)^+$ is determined to be $(1.23 \pm 0.21)\%$, which differs significantly from the theoretical predictions evaluated in Refs. [23, 25] by 1-2 orders of magnitude. A comparable scenario has been seen in $D_s^+ \rightarrow a_0(980)^{+(0)}\pi^{0(+)}$ decay [96]. Nevertheless, that puzzle can be resolved by accounting for a long-distance contribution [97, 98]. However, the BF and line shape eval-

ated from this long-distance effect fail to adequately describe the experimental data of $\Lambda_c^+ \rightarrow \Lambda a_0(980)^+$ decay. Such a large difference between theory and experiment suggests some unknown decay mechanisms. In addition, this large BF implies that Λ_c^+ decays may offer a new window to study the light scalar meson $a_0(980)^+$.

Furthermore, we determine $\mathcal{B}[\Lambda_c^+ \rightarrow \Sigma(1385)^+\eta] = (6.78 \pm 0.58 \pm 0.16 \pm 0.47) \times 10^{-3}$ and $\mathcal{B}[\Lambda_c^+ \rightarrow \Lambda(1670)\pi^+]$. $\mathcal{B}[\Lambda(1670) \rightarrow \Lambda\eta] = (2.74 \pm 0.54 \pm 0.24 \pm 0.18) \times 10^{-3}$, where the third uncertainty of $\mathcal{B}[\Lambda_c^+ \rightarrow \Sigma(1385)^+\eta]$ also includes the uncertainty from $\mathcal{B}[\Sigma(1385)^+ \rightarrow \Lambda\pi^+] = (87.5 \pm 1.5)\%$ [73]. The obtained product $\mathcal{B}[\Lambda_c^+ \rightarrow \Sigma(1385)^+\eta]$ is consistent with the previous BESIII result [60] within 2σ but differs from the Belle result [61] by over 3σ . The obtained $\mathcal{B}[\Lambda_c^+ \rightarrow \Lambda(1670)\pi^+]$. $\mathcal{B}[\Lambda(1670) \rightarrow \Lambda\eta]$ is consistent with the Belle result within 1σ . The $\mathcal{B}[\Lambda_c^+ \rightarrow \Sigma(1385)^+\eta]$ measured in this work is in good agreement with recent calculations [26, 99], while it differs from the early calculations [100, 101] by over 3σ . There is a pure nonfactorizable contribution in $\Lambda_c^+ \rightarrow \Sigma(1385)^+\eta$ [26] that is difficult to calculate; our measurement is crucial to calibrate theoretical treatments of this nonfactorizable contribution. Based on the PWA results, the decay asymmetry parameters of these three intermediate processes are determined for the first time. The measured decay asymmetry parameter of $\Lambda_c^+ \rightarrow \Sigma(1385)^+\eta$, $-0.61 \pm 0.15 \pm 0.04$, is consistent with $-0.97^{+0.43}_{-0.03}$ evaluated in Ref. [99]. However, that of $\Lambda_c^+ \rightarrow \Lambda a_0(980)^+$ is close to -1 , which contradicts the small asymmetry estimated in Ref. [23]. This discrepancy might indicate issues in the consideration of $a_0(980)^+$ decay constant or parity-violating transition amplitudes. Our results are essential to improve the current understanding of the dynamics of the hadronic Λ_c^+ decays.

We thank En Wang, Guan-Ying Wang, Yu-Kuo Hsiao and Jia-Jun Wu for useful discussions. The BESIII Collaboration thanks the staff of BEPCII and the IHEP computing center for their strong support. This work is supported in part by National Key R&D Program of China under Contracts Nos. 2020YFA0406400, 2020YFA0406300, 2023YFA1606000; National Natural Science Foundation of China (NSFC) under Contracts Nos. 11635010, 11735014, 11835012, 11935015, 11935016, 11935018, 11961141012, 12025502, 12035009, 12035013, 12061131003, 12192260, 12192261, 12192262, 12192263, 12192264, 12192265, 12221005, 12225509, 12235017; the Chinese Academy of Sciences (CAS) Large-Scale Scientific Facility Program; the CAS Center for Excellence in Particle Physics (CCEPP); Joint Large-Scale Scientific Facility Funds of the NSFC and CAS under Contract No. U1832207; CAS Key Research Program of Frontier Sciences under Contracts Nos. QYZDJ-SSW-SLH003, QYZDJ-SSW-SLH040; 100 Talents Program of CAS; The Institute of Nuclear and Particle Physics (INPAC) and Shanghai Key Laboratory for Particle Physics and

Cosmology; European Union's Horizon 2020 research and innovation programme under Marie Skłodowska-Curie grant agreement under Contract No. 894790; German Research Foundation DFG under Contracts Nos. 455635585, Collaborative Research Center CRC 1044, FOR5327, GRK 2149; Istituto Nazionale di Fisica Nucleare, Italy; Ministry of Development of Turkey under Contract No. DPT2006K-120470; National Research Foundation of Korea under Contract No. NRF-2022R1A2C1092335; National Science and Technology fund of Mongolia; National Science Research and Innovation Fund (NSRF) via the Program Management Unit for Human Resources & Institutional Development, Research and Innovation of Thailand under Contract No. B16F640076; Polish National Science Centre under Contract No. 2019/35/O/ST2/02907; The Swedish Research Council; U. S. Department of Energy under Contract No. DE-FG02-05ER41374.

-
- [1] M. Gell-Mann, *Phys. Lett.* **8**, 214 (1964).
 - [2] G. Zweig, *CERN Report No. CERN-TH-401*, 1964; *CERN Report No. CERN-TH-412*, 1964.
 - [3] N. Brambilla, S. Eidelman, C. Hanhart, A. Nefediev, C. P. Shen, C. E. Thomas, A. Vairo and C. Z. Yuan, *Phys. Rep.* **873**, 1 (2020).
 - [4] F. K. Guo, C. Hanhart, U. G. Meißner, Q. Wang, Q. Zhao and B. S. Zou, *Rev. Mod. Phys.* **90**, 015004 (2018).
 - [5] S. L. Olsen, T. Skwarnicki and D. Zieminska, *Rev. Mod. Phys.* **90**, 015003 (2018).
 - [6] H. X. Chen, W. Chen, X. Liu and S. L. Zhu, *Phys. Rept.* **639**, 1 (2016).
 - [7] N. Brambilla *et al.*, *Eur. Phys. J. C* **71**, 1534 (2011).
 - [8] E. Klemp and A. Zaitsev, *Phys. Rept.* **454**, 1 (2007).
 - [9] Z. Liu and R. E. Mitchell, *Sci. Bull.* **68**, 2148 (2023).
 - [10] R. Aaij *et al.* (LHCb Collaboration), *Phys. Rev. Lett.* **122**, 222001 (2019).
 - [11] R. Aaij *et al.* (LHCb Collaboration), *Phys. Rev. Lett.* **115**, 072001 (2015).
 - [12] R. Aaij *et al.* (LHCb Collaboration), *JHEP* **09**, 028 (2019).
 - [13] N. R. Soni, A. N. Gadaria, J. J. Patel and J. N. Pandya, *Phys. Rev. D* **102**, 016013 (2020).
 - [14] E. Klemp, *Phys. Lett. B* **820**, 136512 (2021).
 - [15] N. N. Achasov, *Nucl. Phys. A* **675**, 279 (2000).
 - [16] R. L. Jaffe, *Phys. Rept.* **409**, 1 (2005).
 - [17] C. Alexandrou, J. Berlin, M. Dalla Brida, J. Finkenrath, T. Leontiou and M. Wagner, *Phys. Rev. D* **97**, 034506 (2018).
 - [18] J. D. Weinstein and N. Isgur, *Phys. Rev. Lett.* **48**, 659 (1982).
 - [19] G. Janssen, B. C. Pearce, K. Holinde and J. Speth, *Phys. Rev. D* **52**, 2690 (1995).
 - [20] J. A. Oller and E. Oset, *Nucl. Phys. A* **620**, 438 (1997).
 - [21] T. Sekihara and S. Kumano, *Phys. Rev. D* **92**, 034010 (2015).
 - [22] H. A. Ahmed and C. W. Xiao, *Phys. Rev. D* **101**, 094034 (2020).
 - [23] A. Sharma and R. C. Verma, *J. Phys. G* **36**, 075005

- (2009).
- [24] S. Barlag *et al.* (ACCMOR Collaboration), *Z. Phys. C* **48**, 29 (1990).
- [25] Y. Yu and Y. K. Hsiao, *Phys. Lett. B* **820**, 136586 (2021).
- [26] Y. K. Hsiao, Q. Yi, S. T. Cai and H. J. Zhao, *Eur. Phys. J. C* **80**, 1067 (2020).
- [27] G. Y. Wang, N. C. Wei, H. M. Yang, E. Wang, L. S. Geng and J. J. Xie, *Phys. Rev. D* **106**, 056001 (2022).
- [28] E. Wang, L. S. Geng, J. J. Wu, J. J. Xie and B. S. Zou, *Chin. Phys. Lett.* **41**, 101401 (2024).
- [29] C. Helminen and D. O. Riska, *Nucl. Phys. A* **699**, 624 (2002).
- [30] A. Zhang, Y. R. Liu, P. Z. Huang, W. Z. Deng, X. L. Chen and S. L. Zhu, *High Energy Phys. Nucl. Phys.* **29** 250 (2005).
- [31] B. S. Zou, *Eur. Phys. J. A* **35**, 325 (2008).
- [32] N. Kaiser, P. B. Siegel and W. Weise, *Phys. Lett. B* **362**, 23 (1995).
- [33] D. Jido, J. A. Oller, E. Oset, A. Ramos and U. G. Meissner, *Nucl. Phys. A* **725**, 181 (2003).
- [34] J. J. Wu, S. Dulat and B. S. Zou, *Phys. Rev. D* **80**, 017503 (2009).
- [35] K. P. Khemchandani, A. Martinez Torres, H. Kaneko, H. Nagahiro and A. Hosaka, *Phys. Rev. D* **84**, 094018 (2011).
- [36] J. J. Wu, S. Dulat and B. S. Zou, *Phys. Rev. C* **81**, 045210 (2010).
- [37] P. Gao, B. S. Zou and A. Sibirtsev, *Nucl. Phys. A* **867**, 41 (2011).
- [38] K. P. Khemchandani, A. Martínez Torres and J. A. Oller, *Phys. Rev. C* **100**, 015208 (2019).
- [39] Y. L. Pan and F. L. Forman, *Phys. Rev. Lett.* **23**, 806 (1969).
- [40] Y. L. Pan and F. L. Forman, *Phys. Rev. Lett.* **23**, 808 (1969).
- [41] S. Chekanov *et al.* (ZEUS Collaboration), *Phys. Lett. B* **591**, 7 (2004).
- [42] I. Zychor, V. Koptev, M. Buscher, A. Dzyuba, I. Keshelashvili, V. Kleber, H. R. Koch, S. Krewald, Y. Maeda and S. Mikirtichyan, *et al.* *Phys. Rev. Lett.* **96**, 012002 (2006).
- [43] P. Gao, J. J. Wu and B. S. Zou, *Phys. Rev. C* **81**, 055203 (2010).
- [44] K. Moriya *et al.* (CLAS Collaboration), *Phys. Rev. C* **87**, 035206 (2013).
- [45] Y. H. Chen and B. S. Zou, *Phys. Rev. C* **88**, 024304 (2013).
- [46] L. Roca and E. Oset, *Phys. Rev. C* **88**, 055206 (2013).
- [47] S. H. Kim, K. P. Khemchandani, A. Martinez Torres, S. i. Nam and A. Hosaka, *Phys. Rev. D* **103**, 114017 (2021).
- [48] Y. H. Lyu, H. Zhang, N. C. Wei, B. C. Ke, E. Wang and J. J. Xie, *Chin. Phys. C* **47**, 053108 (2023).
- [49] E. Wang, J. J. Xie and E. Oset, *Phys. Lett. B* **753**, 526 (2016).
- [50] L. J. Liu, E. Wang, J. J. Xie, K. L. Song and J. Y. Zhu, *Phys. Rev. D* **98**, 114017 (2018).
- [51] Y. Ma *et al.* (Belle Collaboration), *Phys. Rev. Lett.* **130**, 151903 (2023).
- [52] B. Dey *et al.* (CLAS Collaboration), *Phys. Rev. C* **89**, 055208 (2014).
- [53] R. F. Lebed, *Phys. Rev. D* **92**, 114030 (2015).
- [54] B. Pal *et al.* (Belle Collaboration), *Phys. Rev. D* **96**, 051102 (2017).
- [55] J. J. Xie and F. K. Guo, *Phys. Lett. B* **774**, 108 (2017).
- [56] X. Liu, H. Huang and J. Ping, *Phys. Rev. C* **98**, 055203 (2018).
- [57] J. J. Xie, L. S. Geng and F. K. Guo, *EPJ Web Conf.* **241**, 02010 (2020).
- [58] J. J. Xie and L. S. Geng, *Phys. Rev. D* **95**, 074024 (2017).
- [59] W. T. Lyu, S. C. Zhang, G. Y. Wang, J. J. Wu, E. Wang, L. S. Geng and J. J. Xie, *Phys. Rev. D* **110**, 054020 (2024).
- [60] M. Ablikim *et al.* (BESIII Collaboration), *Phys. Rev. D* **99**, 032010 (2019).
- [61] J. Y. Lee *et al.* (Belle Collaboration), *Phys. Rev. D* **103**, 052005 (2021).
- [62] M. Ablikim *et al.* (BESIII Collaboration), *Chin. Phys. C* **39**, 093001 (2015).
- [63] M. Ablikim *et al.* (BESIII Collaboration), *Chin. Phys. C* **40**, 063001 (2016).
- [64] M. Ablikim *et al.* (BESIII Collaboration), *Chin. Phys. C* **46**, 113002 (2022).
- [65] M. Ablikim *et al.* (BESIII Collaboration), *Chin. Phys. C* **46**, 113003 (2022).
- [66] B. C. Ke, J. Koponen, H. B. Li and Y. Zheng, *Ann. Rev. Nucl. Part. Sci.* **73**, 285 (2023).
- [67] M. Ablikim *et al.* (BESIII Collaboration), *Nucl. Instrum. Meth. A* **614**, 345 (2010).
- [68] C. H. Yu *et al.*, Proceedings of IPAC2016, Busan, Korea, 2016.
- [69] M. Ablikim *et al.* (BESIII Collaboration), *Chin. Phys. C* **44**, 040001 (2020).
- [70] K. X. Huang, *et al.*, *Nucl. Sci. Tech.* **33**, 142 (2022).
- [71] H. B. Li and X. R. Lyu, *Natl. Sci. Rev.* **8**, nwab181 (2021).
- [72] M. Ablikim *et al.* (BESIII Collaboration), *JHEP* **12**, 033 (2022).
- [73] R.L. Workman *et al.* (Particle Data Group), *Prog. Theor. Exp. Phys.* **2022**, 083C01 (2022) and 2023 update.
- [74] T. Hastie, R. Tibshirani, and J. Friedman, Springer, New York, NY, 2009.
- [75] H. Voss, A. Hocker, J. Stelzer and F. Tegenfeldt, *PoS ACAT*, 040 (2007).
- [76] See Supplemental Material at [URL will be inserted by publisher], which includes Refs. [77–80], for additional details of the analysis.
- [77] S. U. Chung, *Phys. Rev. D* **48**, 1225 (1993).
- [78] S. U. Chung, *Phys. Rev. D* **57**, 431 (1998).
- [79] S. U. Chung, *Int. J. Mod. Phys. A* **18**, 457 (2003).
- [80] F. Von Hippel and C. Quigg, *Phys. Rev. D* **5**, 624 (1972).
- [81] M. Pivk and F. R. Le Diberder, *Nucl. Instrum. Meth. A* **555**, 356 (2005).
- [82] S. U. Chung, “Spin Formalisms”, CERN-1971-008.
- [83] J. D. Richman, “An Experimenter’s Guide to the Helicity Formalism”, CALT-68-1148
- [84] Y. Jiang *et al.*, A partial wave analysis program using tensorflow tf-pwa.
- [85] H. Chen and R. G. Ping, *Phys. Rev. D* **99**, 114027 (2019).
- [86] M. Ablikim *et al.* (BESIII Collaboration), *Phys. Rev. Lett.* **120**, 132001 (2018).
- [87] M. Ablikim *et al.* (BESIII Collaboration), *Phys. Rev. Lett.* **131**, 191901 (2023).
- [88] S. M. Flatté, *Phys. Lett. B* **63**, 224 (1976).
- [89] M. Ablikim *et al.* (BESIII Collaboration), *Phys. Rev. D* **95**, 032002 (2017).
- [90] A. V. Sarantsev, M. Matveev, V. A. Nikonov, A. V. Anisovich, U. Thoma and E. Klempf, *Eur. Phys.*

- J. A **55**, 180 (2019).
- [91] M. Wang, Y. Jiang, Y. Liu, W. Qian, X. Lyu and L. Zhang, Chin. Phys. C **45**, 063103 (2021).
- [92] C. Langenbruch, Eur. Phys. J. C **82**, 393 (2022).
- [93] H. Albrecht *et al.* (ARGUS Collaboration), Phys. Lett. B **241**, 278 (1990).
- [94] M. Ablikim *et al.* (BESIII Collaboration), Phys. Rev. D **109**, 032003 (2024).
- [95] If only two coupled channels, $K\bar{K}$ and $\eta\pi$, are considered, one can use the partial width ratio $\Gamma[a_0(980) \rightarrow K\bar{K}]/\Gamma[a_0(980) \rightarrow \eta\pi] = 0.172 \pm 0.019$ [73] to calculate $\mathcal{B}[a_0(980) \rightarrow \eta\pi] = 0.853 \pm 0.014$.
- [96] M. Ablikim *et al.* (BESIII Collaboration), Phys. Rev. Lett. **123**, 112001 (2019).
- [97] Y. K. Hsiao, Y. Yu and B. C. Ke, Eur. Phys. J. C **80**, 895 (2020).
- [98] R. Molina, J. J. Xie, W. H. Liang, L. S. Geng and E. Oset, Phys. Lett. B **803**, 135279 (2020).
- [99] C. Q. Geng, C. W. Liu, T. H. Tsai and Y. Yu, Phys. Rev. D **99**, 114022 (2019).
- [100] J. G. Korner and M. Kramer, Z. Phys. C **55**, 659 (1992).
- [101] K. K. Sharma and R. C. Verma, Phys. Rev. D **55**, 7067 (1997).

Supplemental Material for “Observation of $\Lambda_c^+ \rightarrow \Lambda a_0(980)^+$ and Evidence for $\Sigma(1380)^+$ in $\Lambda_c^+ \rightarrow \Lambda\pi^+\eta$ ”

Fit results for different PWA samples

Table III summarizes the results of the M_{BC} fits to the data from different c.m. energies. The individual fits are shown in Fig. 4.

TABLE III. The results of fits to M_{BC} distributions from different energy points, along with M_{BC} signal regions, signal yields, and signal purities for the $\eta \rightarrow \gamma\gamma$ and $\eta \rightarrow \pi^+\pi^-\pi^0$ channels. The uncertainties are statistical only.

Sample (MeV)	M_{BC} (GeV/ c^2)	$\eta \rightarrow \gamma\gamma$		$\eta \rightarrow \pi^+\pi^-\pi^0$	
		Yields	Purities (%)	Yields	Purities (%)
4600	(2.282, 2.291)	131 ± 12	86.2 ± 1.5	27 ± 6	85.6 ± 3.9
4612	(2.282, 2.291)	15 ± 5	77.8 ± 6.8	3 ± 1	93.5 ± 4.3
4628	(2.282, 2.291)	89 ± 11	77.1 ± 2.8	21 ± 5	88.8 ± 3.7
4641	(2.282, 2.292)	95 ± 11	77.2 ± 2.8	26 ± 6	87.8 ± 3.5
4661	(2.282, 2.292)	92 ± 11	82.0 ± 2.2	24 ± 5	87.9 ± 3.6
4682	(2.281, 2.293)	265 ± 19	77.0 ± 1.6	50 ± 8	81.8 ± 3.2
4700	(2.279, 2.293)	78 ± 10	77.2 ± 3.0	16 ± 5	80.8 ± 5.8
4740	(2.281, 2.296)	17 ± 5	73.5 ± 6.9	2 ± 2	49.1 ± 29.8
4750	(2.281, 2.296)	33 ± 7	67.6 ± 5.4	10 ± 3	87.4 ± 5.2
4781	(2.279, 2.297)	60 ± 9	76.8 ± 3.3	10 ± 4	74.7 ± 8.2
4843	(2.279, 2.297)	37 ± 7	74.5 ± 4.4	7 ± 3	72.4 ± 10.1

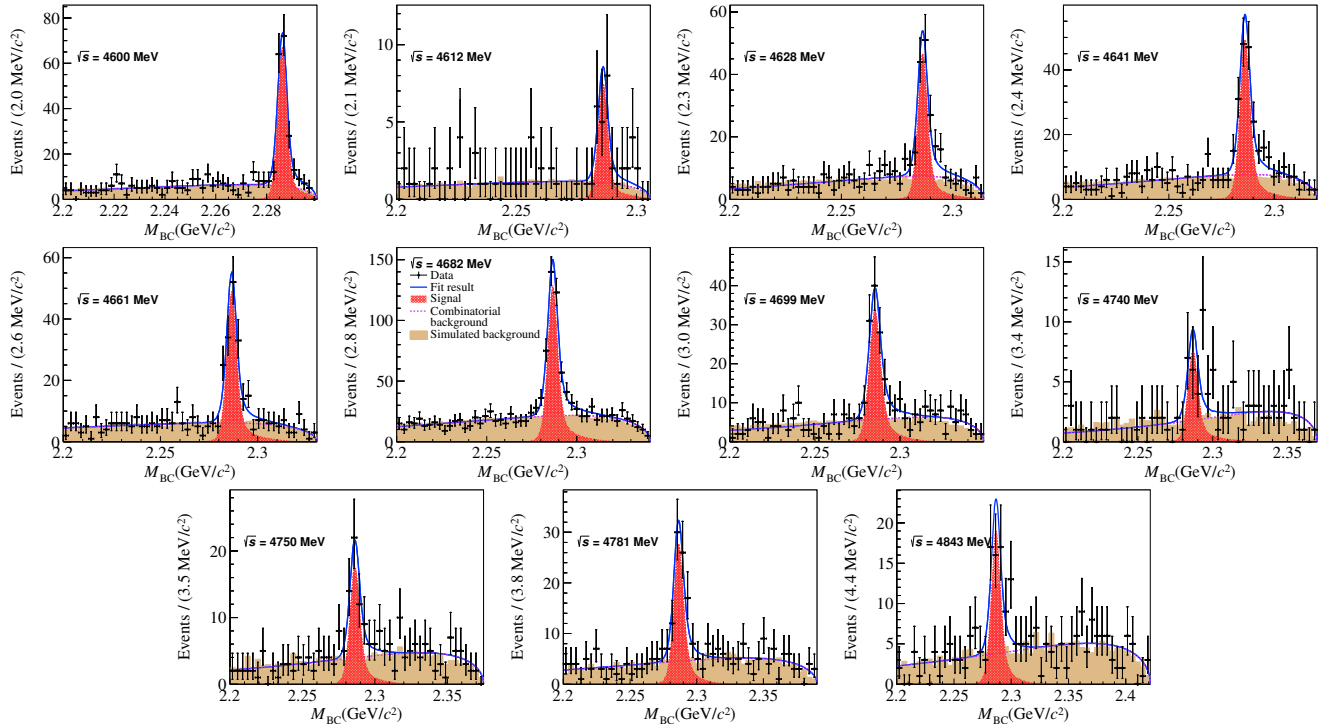


FIG. 4. The fits to the M_{BC} distributions for $\eta \rightarrow \gamma\gamma$ and $\eta \rightarrow \pi^+\pi^-\pi^0$ channels combined from the different energy points. The points with error bars are data, the brown solid histograms are MC-simulated background, the red hatched histograms are signal, the violet dashed lines are background shapes, and the blue lines show the total fit.

Helicity amplitude definition

In helicity amplitude formalism, three-body decay is described as a two-step sequential quasi-two-body decay based on isobar model. For each two-body decay $0 \rightarrow 1 + 2$, the helicity amplitude can be written as $A_{\lambda_0, \lambda_1, \lambda_2}^{0 \rightarrow 1+2} = H_{\lambda_1, \lambda_2}^{0 \rightarrow 1+2} D_{\lambda_0, \lambda_1 - \lambda_2}^{J_0*}(\phi, \theta, 0)$, where the helicity coupling $H_{\lambda_1, \lambda_2}^{0 \rightarrow 1+2}$ is given by the LS coupling formula [1–3] along with barrier factor terms

$$H_{\lambda_1, \lambda_2}^{0 \rightarrow 1+2} = \sum_{ls} g_{ls} \sqrt{\frac{2l+1}{2J_0+1}} \langle l0, s\delta | J_0, \delta \rangle \times \langle J_1 J_2, \lambda_1 - \lambda_2 | s, \delta \rangle \left(\frac{q}{q_0}\right)^l B'_l(q, q_0, d), \quad (1)$$

and $D_{\lambda_0, \lambda_1 - \lambda_2}^{J_0*}$ is the Wigner D -function, ϕ and θ are helicity angles. The g_{ls} is the partial wave amplitude, $J_{0,1,2}$ are the spins of the particles 0, 1, and 2, $\lambda_{1,2}$ are the helicities for the particles 1 and 2, and $\delta = \lambda_1 - \lambda_2$ is the helicity difference. Here, q is the three-momentum modulus of particle 1 in the rest frame of particle 0, which is calculated as $q = \sqrt{\frac{[m^2 - (m_1 + m_2)^2][m^2 - (m_1 - m_2)^2]}{2m}}$, where m , m_1 and m_2 are the masses of the particles 0, 1, and 2, respectively. The normalization factor q_0 is calculated at the nominal resonance mass. The factor $B'_l(q, q_0, d)$ is the reduced Blatt-Weisskopf barrier factor [4], which is explicitly expressed as

$$\begin{aligned} B'_0(q, q_0, d) &= 1, \\ B'_1(q, q_0, d) &= \sqrt{\frac{1 + (q_0 d)^2}{1 + (qd)^2}}, \\ B'_2(q, q_0, d) &= \sqrt{\frac{9 + 3(q_0 d)^2 + (q_0 d)^4}{9 + 3(qd)^2 + (qd)^4}}, \end{aligned} \quad (2)$$

and the radius of the centrifugal barrier d is chosen as $d = 0.73$ fm [5]. For decay chains with resonant intermediate states, the barrier factor term is included. For those with NR intermediate states, the barrier factor term is omitted.

The $\Lambda_c^+ \rightarrow \Lambda a_0(980)^+, a_0(980)^+ \rightarrow \pi^+ \eta, \Lambda \rightarrow p \pi^-$ decay amplitude is constructed as

$$A_{\lambda_{\Lambda_c^+}, \lambda_p}^{a_0^+} = \sum_{\lambda_\Lambda} A_{\lambda_{\Lambda_c^+}, 0, \lambda_\Lambda}^{\Lambda_c^+ \rightarrow a_0^+ \Lambda} R_{a_0^+}(M_{\pi^+ \eta}) A_{0, 0, 0}^{a_0^+ \rightarrow \pi^+ \eta} A_{\lambda_\Lambda, \lambda_p, 0}^{\Lambda \rightarrow p \pi^-}, \quad (3)$$

where $R_{a_0^+}$ is the propagator of the $a_0(980)^+$ described by the two coupled-channel Flatté model [6],

$$R_{a_0^+}(m) = \frac{1}{m_0^2 - m^2 - i(g_1 \rho_{\eta \pi}(m) + g_2 \rho_{K \bar{K}}(m))}. \quad (4)$$

The nominal mass m_0 and coupling constants of the $a_0(980)^+$ decaying to the $\eta \pi$, g_1 , and $K \bar{K}$, g_2 , coupled channels are quoted from Ref. [7]. For the NR decay, the dynamical function is set to be unity, so the decay amplitude is

$$A_{\lambda_{\Lambda_c^+}, \lambda_p}^{NR} = \sum_{\lambda_\Lambda} A_{\lambda_{\Lambda_c^+}, 0, \lambda_\Lambda}^{\Lambda_c^+ \rightarrow NR \Lambda}(M_{\pi^+ \eta}) A_{0, 0, 0}^{NR \rightarrow \pi^+ \eta} A_{\lambda_\Lambda, \lambda_p, 0}^{\Lambda \rightarrow p \pi^-}. \quad (5)$$

For the decay through the Σ^{*+} and Λ^* intermediate states, the amplitudes are written as

$$A_{\lambda_{\Lambda_c^+}, \lambda_p}^{\Sigma^{*+}} = \sum_{\lambda_{\Sigma^{*+}}, \lambda_\Lambda} A_{\lambda_{\Lambda_c^+}, \lambda_{\Sigma^{*+}}, 0}^{\Lambda_c^+ \rightarrow \Sigma^{*+} \eta} R_{\Sigma^{*+}}(M_{\Lambda \pi^+}) A_{\lambda_{\Sigma^{*+}}, \lambda_\Lambda, 0}^{\Sigma^{*+} \rightarrow \Lambda \pi^+} A_{\lambda_\Lambda, \lambda_p, 0}^{\Lambda \rightarrow p \pi^-}, \quad (6)$$

$$A_{\lambda_{\Lambda_c^+}, \lambda_p}^{\Lambda^*} = \sum_{\lambda_{\Lambda^*}, \lambda_\Lambda} A_{\lambda_{\Lambda_c^+}, \lambda_{\Lambda^*}, 0}^{\Lambda_c^+ \rightarrow \Lambda^* \pi^+} R_{\Lambda^*}(M_{\Lambda \eta}) A_{\lambda_{\Lambda^*}, \lambda_\Lambda, 0}^{\Lambda^* \rightarrow \Lambda \eta} A_{\lambda_\Lambda, \lambda_p, 0}^{\Lambda \rightarrow p \pi^-}. \quad (7)$$

Here, the relativistic Breit-Wigner (RBW) formula [5] is used as the propagator,

$$R_{\Sigma^{*+}/\Lambda^*} = \frac{1}{m_0^2 - m^2 - im_0 \Gamma(m)}. \quad (8)$$

The nominal mass and width of the $\Sigma(1385)^+$ are fixed to the corresponding values from the PDG [8], and those of $\Lambda(1670)$ are taken from a recent measurement [9]. The amplitude of $\Lambda \rightarrow p\pi^-$ is constrained according to

$$\alpha_\Lambda = \frac{\left| H_{\frac{1}{2},0}^{\Lambda \rightarrow p\pi^-} \right|^2 - \left| H_{-\frac{1}{2},0}^{\Lambda \rightarrow p\pi^-} \right|^2}{\left| H_{\frac{1}{2},0}^{\Lambda \rightarrow p\pi^-} \right|^2 + \left| H_{-\frac{1}{2},0}^{\Lambda \rightarrow p\pi^-} \right|^2} = -\frac{2 \operatorname{Re} \left(g_{0,\frac{1}{2}}^{\Lambda \rightarrow p\pi^-} g_{1,\frac{1}{2}}^{\Lambda \rightarrow p\pi^- *} \right)}{\left| g_{0,\frac{1}{2}}^{\Lambda \rightarrow p\pi^-} \right|^2 + \left| g_{1,\frac{1}{2}}^{\Lambda \rightarrow p\pi^-} \right|^2}, \quad (9)$$

where α_Λ is the decay asymmetry taken from the PDG [8]. The full amplitude of Λ_c^+ decay is the coherent sum of amplitudes of all decay chains, and the alignment D -functions are considered to align the helicities of the final state protons [10, 11],

$$\mathcal{A}_{\lambda_{\Lambda_c^+}, \lambda_p} = A_{\lambda_{\Lambda_c^+}, \lambda_p}^{a_0^+} + A_{\lambda_{\Lambda_c^+}, \lambda_p}^{NR} + \sum_{\lambda'_p} A_{\lambda_{\Lambda_c^+}, \lambda_p}^{\Sigma^{**+}} D_{\lambda'_p, \lambda_p}(\alpha_p, \beta_p, \gamma_p) + \sum_{\lambda'_p} A_{\lambda_{\Lambda_c^+}, \lambda_p}^{\Lambda^*} D_{\lambda'_p, \lambda_p}(\alpha'_p, \beta'_p, \gamma'_p). \quad (10)$$

The total amplitude for polarized Λ_c^+ can be written as

$$\begin{aligned} |\mathcal{A}|^2 &= \sum_{\lambda_{\Lambda_c^+}, \lambda'_{\Lambda_c^+}, \lambda_p} \rho_{\lambda_{\Lambda_c^+}, \lambda'_{\Lambda_c^+}, \lambda_p} \mathcal{A}_{\lambda_{\Lambda_c^+}, \lambda_p} \mathcal{A}_{\lambda_{\Lambda_c^+}, \lambda_p}^* \\ &= \sum_{\lambda_p} \left[(\mathcal{A}_{-1/2, \lambda_p} \mathcal{A}_{1/2, \lambda_p}) \cdot \frac{1}{2} \begin{pmatrix} 1 + P_z & P_x - iP_y \\ P_x + iP_y & 1 - P_z \end{pmatrix} \cdot \begin{pmatrix} \mathcal{A}_{-1/2, \lambda_p}^* \\ \mathcal{A}_{1/2, \lambda_p}^* \end{pmatrix} \right], \end{aligned} \quad (11)$$

where P_x, P_y, P_z are the polarization components. According to Ref. [12], the polarization components of Λ_c^+ from e^+e^- collision are fixed to $P_z = P_x = 0$, $P_y(\theta_{ee}, \alpha_0, \Delta_0) \propto \sqrt{1 - \alpha_0^2} \sin \theta_{ee} \cos \theta_{ee} \sin \Delta_0$. Here, θ_{ee} is the polar angle of the Λ_c^+ with respect to the e^+ beam in the e^+e^- c.m. system, α_0 is fixed to the values from Refs. [13, 14], and Δ_0 is fixed according to polarization results in data. The α_0 and Δ_0 have a relation with helicity amplitudes for $e^+e^- \rightarrow \Lambda_c^+ \bar{\Lambda}_c^-$,

$$\begin{aligned} \alpha_0 &= \frac{|H_{\frac{1}{2}, -\frac{1}{2}}^{e^+e^- \rightarrow \Lambda_c^+ \bar{\Lambda}_c^-}|^2 - 2|H_{\frac{1}{2}, \frac{1}{2}}^{e^+e^- \rightarrow \Lambda_c^+ \bar{\Lambda}_c^-}|^2}{|H_{\frac{1}{2}, -\frac{1}{2}}^{e^+e^- \rightarrow \Lambda_c^+ \bar{\Lambda}_c^-}|^2 + 2|H_{\frac{1}{2}, \frac{1}{2}}^{e^+e^- \rightarrow \Lambda_c^+ \bar{\Lambda}_c^-}|^2}, \\ \Delta_0 &= \arg(H_{\frac{1}{2}, -\frac{1}{2}}^{e^+e^- \rightarrow \Lambda_c^+ \bar{\Lambda}_c^-}) - \arg(H_{\frac{1}{2}, \frac{1}{2}}^{e^+e^- \rightarrow \Lambda_c^+ \bar{\Lambda}_c^-}). \end{aligned} \quad (12)$$

Definitions of decay asymmetry parameters

The explicit definitions of the decay asymmetry parameters are given below.

$$\alpha_{\Lambda a_0(980)^+} = \frac{\left| H_{\frac{1}{2},0}^{\Lambda_c^+ \rightarrow \Lambda a_0(980)^+} \right|^2 - \left| H_{-\frac{1}{2},0}^{\Lambda_c^+ \rightarrow \Lambda a_0(980)^+} \right|^2}{\left| H_{\frac{1}{2},0}^{\Lambda_c^+ \rightarrow \Lambda a_0(980)^+} \right|^2 + \left| H_{-\frac{1}{2},0}^{\Lambda_c^+ \rightarrow \Lambda a_0(980)^+} \right|^2} = -\frac{2 \operatorname{Re} \left(g_{0,\frac{1}{2}}^{\Lambda_c^+ \rightarrow \Lambda a_0(980)^+} g_{1,\frac{1}{2}}^{\Lambda_c^+ \rightarrow \Lambda a_0(980)^+ *} \right)}{\left| g_{0,\frac{1}{2}}^{\Lambda_c^+ \rightarrow \Lambda a_0(980)^+} \right|^2 + \left| g_{1,\frac{1}{2}}^{\Lambda_c^+ \rightarrow \Lambda a_0(980)^+} \right|^2}, \quad (13)$$

$$\alpha_{\Sigma(1385)^+ \eta} = \frac{\left| H_{\frac{1}{2},0}^{\Lambda_c^+ \rightarrow \Sigma(1385)^+ \eta} \right|^2 - \left| H_{-\frac{1}{2},0}^{\Lambda_c^+ \rightarrow \Sigma(1385)^+ \eta} \right|^2}{\left| H_{\frac{1}{2},0}^{\Lambda_c^+ \rightarrow \Sigma(1385)^+ \eta} \right|^2 + \left| H_{-\frac{1}{2},0}^{\Lambda_c^+ \rightarrow \Sigma(1385)^+ \eta} \right|^2} = -\frac{2 \operatorname{Re} \left(g_{1,\frac{3}{2}}^{\Lambda_c^+ \rightarrow \Sigma(1385)^+ \eta} g_{2,\frac{3}{2}}^{\Lambda_c^+ \rightarrow \Sigma(1385)^+ \eta *} \right)}{\left| g_{1,\frac{3}{2}}^{\Lambda_c^+ \rightarrow \Sigma(1385)^+ \eta} \right|^2 + \left| g_{2,\frac{3}{2}}^{\Lambda_c^+ \rightarrow \Sigma(1385)^+ \eta} \right|^2}, \quad (14)$$

$$\alpha_{\Lambda(1670)\pi^+} = \frac{\left| H_{\frac{1}{2},0}^{\Lambda_c^+ \rightarrow \Lambda(1670)\pi^+} \right|^2 - \left| H_{-\frac{1}{2},0}^{\Lambda_c^+ \rightarrow \Lambda(1670)\pi^+} \right|^2}{\left| H_{\frac{1}{2},0}^{\Lambda_c^+ \rightarrow \Lambda(1670)\pi^+} \right|^2 + \left| H_{-\frac{1}{2},0}^{\Lambda_c^+ \rightarrow \Lambda(1670)\pi^+} \right|^2} = -\frac{2 \operatorname{Re} \left(g_{0,\frac{1}{2}}^{\Lambda_c^+ \rightarrow \Lambda(1670)\pi^+} g_{1,\frac{1}{2}}^{\Lambda_c^+ \rightarrow \Lambda(1670)\pi^+ *} \right)}{\left| g_{0,\frac{1}{2}}^{\Lambda_c^+ \rightarrow \Lambda(1670)\pi^+} \right|^2 + \left| g_{1,\frac{1}{2}}^{\Lambda_c^+ \rightarrow \Lambda(1670)\pi^+} \right|^2}. \quad (15)$$

Dalitz plots for the data and the baseline solution

Dalitz plots for both the data and the baseline solution fit are shown in Fig. 5.

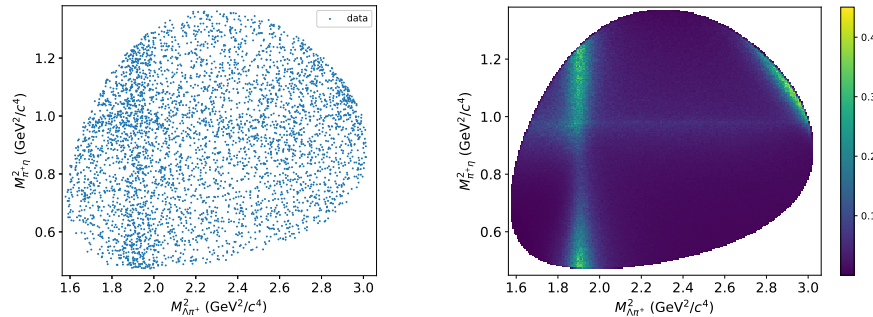


FIG. 5. The Dalitz plots of data (left) and fit results (right) at all energy points.

Fit results of PWA with $\Sigma(1380)^+$

In the $a_0(980)^+$ signal region in Dalitz plot, defined as $M_{\Lambda\pi^+} > 1.44 \text{ GeV}/c^2$ and $M_{\Lambda\eta} > 1.72 \text{ GeV}/c^2$, the Σ^{*+} helicity angle, $\cos \theta_{\Sigma^{*+}}$ distribution are shown in Fig. 6. It is found that in the baseline model, the fit curve exceeds the data near $\cos \theta_{\Sigma^{*+}} \simeq -0.35$. However, in model A where the NR_{0+} amplitude is replaced by the $\Sigma(1380)^+$, the fit curve is more consistent with data.

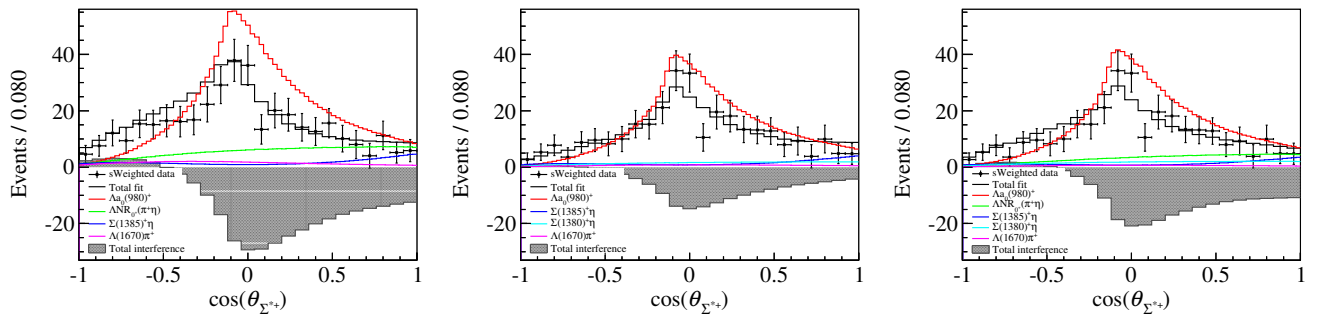


FIG. 6. Projections of the fit results vs. the Σ^{*+} helicity angle, $\cos \theta_{\Sigma^{*+}}$ in the baseline model (left), model A (middle), and model B (right). The points with error bars are sWeighted data at all energy points. The curves in different colors are different components.

Test $\Lambda(1670)$ and $a_0(980)^+$ line-shapes of FSI model

Alternative PWA fits are performed by replacing the RBW and Flatté model with the FSI model [15]. Figure 7 (a) shows the projection in the $M_{\Lambda\eta}$ spectrum utilizing a $\Lambda(1670)$ FSI model. Figure 7 (b) and (c) show the projections in the $M_{\pi^+\eta}$ spectrum exploiting the $a_0(980)^+$ FSI model with and without including a NR component. It is found that if NR and $a_0(980)^+$ FSI are both included, the interference is very large. However, an $a_0(980)^+$ FSI without NR cannot describe the $M_{\pi^+\eta}$ spectrum well.

Systematic uncertainties in PWA

The systematic uncertainties of the observables in the PWA are now described. The following sources are considered: fixed parameters, barrier radius, additional resonances, Λ_c^+ polarization, fit methods, data-MC differences, and background modeling. All the systematic uncertainties are listed in Table IV.

Fixed parameters. The uncertainties due to fixed resonance parameters and the Λ decay asymmetry parameter are estimated by varying the fixed values within $\pm 1\sigma$ and re-fitting the data. The quadratic sums of the largest variations from each parameter are assigned as systematic uncertainties.

Barrier radius. The systematic uncertainties of the barrier radius d is determined by setting d to the alternative values derived from Ref. [5], $d = 0.53 \text{ fm}$ and $d = 1.16 \text{ fm}$, which is a $\pm 1\sigma$ region. The fit procedure is repeated, and

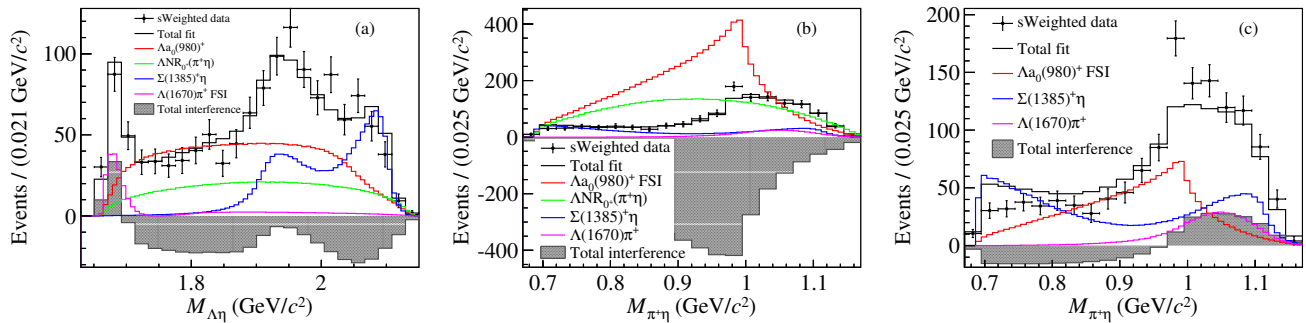


FIG. 7. Projections of the fit results using FSI model in the $M_{\Lambda\eta}$ and $M_{\pi^+\eta}$ spectra. Points with error bars are sWeighted data at all energy points. The curves in different colors are different components.

TABLE IV. Systematic uncertainties (in units of corresponding statistical uncertainties. For $\alpha_{\Lambda a_0(980)^+}$, the symmetric statistical uncertainty 0.12 is used.) on the FFs of $a_0(980)^+$, $\Sigma(1385)^+$ and $\Lambda(1670)$, and the corresponding decay asymmetry parameters $\alpha_{\Lambda a_0(980)^+}$, $\alpha_{\Sigma(1385)^+\eta}$ and $\alpha_{\Lambda(1670)\pi^+}$. The total systematic uncertainties are obtained by summing up all contributions in quadrature.

	$FF_{a_0(980)^+}$	$FF_{\Sigma(1385)^+}$	$FF_{\Lambda(1670)}$	$\alpha_{\Lambda a_0(980)^+}$	$\alpha_{\Sigma(1385)^+\eta}$	$\alpha_{\Lambda(1670)\pi^+}$
Fixed parameters	0.09	0.10	0.32	0.08	0.05	0.11
Barrier radius	0.16	0.08	0.07	0.11	0.09	0.03
Additional resonances	0.21	0.21	0.25	0.14	0.12	1.19
Λ_c^+ polarization	0.05	0.05	0.02	0.06	0.02	0.02
Fit methods	0.07	0.07	0.05	0.09	0.06	0.11
Data-MC differences	0.09	0.01	0.15	0.04	0.08	0.09
Background modeling	0.06	0.06	0.02	0.61	0.19	0.30
Total	0.31	0.27	0.44	0.66	0.27	1.24

the largest variations are assigned as systematic uncertainties.

Additional resonances. The systematic uncertainties associated with additional resonances are considered by adding an additional resonance, the $\Sigma(1660)^+$, which, at 4.3σ , is the most significant among the unused resonances. The fit procedure is repeated, and the changes on the fit results are assigned as the systematic uncertainties.

Λ_c^+ Polarization. To estimate the systematic uncertainties due to the Λ_c^+ polarization, the fixed parameters, *i.e.*, α_0 and Δ_0 , are varied by $\pm 1\sigma$, and the fit procedure is repeated. The largest variations are added in quadrature and assigned as systematic uncertainties.

Fit method. To estimate the potential bias effect due to fit method, we use the results of pull distribution check. For those parameters which are corrected, the uncertainties on the corrections are propagated to obtain systematic uncertainties, and for those parameters which are not corrected, the deviations from 0 (1) in mean (width) are propagated. The total systematic uncertainties are the quadrature sum of mean and width effects.

Data-MC differences. To estimate the systematic uncertainties due to the difference between the MC-determined efficiency and the true one, the effects from tracking and PID of the π^\pm candidates, and the reconstruction of the Λ and η, π^0 candidates are considered. The reconstruction efficiency differences between data and MC simulations have been studied, for example by using $J/\psi \rightarrow p\bar{p}\pi^+\pi^-$ control samples for π^\pm tracking and PID, $\psi(3686) \rightarrow J/\psi\pi^0\pi^0$ and $e^+e^- \rightarrow \omega\pi^0$ control samples for η, π^0 reconstruction, and $J/\psi \rightarrow \bar{p}K^+\Lambda$ for Λ reconstruction. The correction factors $w = \varepsilon_{\text{Data}}/\varepsilon_{\text{MC}}$ are assigned as the weighting factors for the PHSP signal MC sample, and the fit procedure is repeated. The resulting variations on the final results are considered as systematic uncertainties.

Background modeling. To estimate systematic uncertainties due to background description, we change from the sWeight method to a sideband method, in which the events in the M_{BC} sideband region, $[2.20, 2.27] \text{ GeV}/c^2$, are used to model the background shape in the M_{BC} signal regions shown in Table III. The fit procedure is repeated, and the changes in the fit results are taken into account as systematic uncertainties.

Fit results for the BF measurement

The average detection efficiency is defined as

$$\varepsilon = \frac{\sum_i N_{\Lambda_c^+ \bar{\Lambda}_c^-}^i \varepsilon^i}{\sum_i N_{\Lambda_c^+ \bar{\Lambda}_c^-}^i}, \quad (16)$$

where $N_{\Lambda_c^+ \bar{\Lambda}_c^-}^i$ and ε^i are shown in Table V. The average detection efficiencies are $(13.73 \pm 0.02)\%$ and $(4.83 \pm 0.01)\%$ for the $\eta \rightarrow \gamma\gamma$ and $\eta \rightarrow \pi^+\pi^-\pi^0$ channels, respectively. The result of the fit to the M_{BC} distribution combined from the $\eta \rightarrow \gamma\gamma$ and $\eta \rightarrow \pi^+\pi^-\pi^0$ channels at every energy point is shown in Fig. 8.

TABLE V. The results of the simultaneous fit to different energy points, along with the numbers of $\Lambda_c^+ \bar{\Lambda}_c^-$ pairs ($N_{\Lambda_c^+ \bar{\Lambda}_c^-}$), detection efficiencies (ε), the ratios of matched events to mismatched signal yields (r) and the signal yields (N_{sig}) in the $\eta \rightarrow \gamma\gamma$ and $\eta \rightarrow \pi^+\pi^-\pi^0$ channels. The uncertainties are statistical only.

Sample	$N_{\Lambda_c^+ \bar{\Lambda}_c^-}$	$\eta \rightarrow \gamma\gamma$			$\eta \rightarrow \pi^+\pi^-\pi^0$		
		ε (%)	r (%)	N_{sig}	ε (%)	r (%)	N_{sig}
4600	99245 ± 3667	15.69 ± 0.05	5.41 ± 0.08	152.1 ± 5.2	5.76 ± 0.03	20.50 ± 0.29	32.3 ± 1.1
4612	17434 ± 833	14.65 ± 0.08	5.69 ± 0.14	24.9 ± 0.9	5.02 ± 0.05	17.87 ± 0.45	4.9 ± 0.2
4628	89286 ± 3348	14.44 ± 0.05	5.70 ± 0.09	125.9 ± 4.3	4.71 ± 0.03	17.48 ± 0.30	23.8 ± 0.8
4641	95435 ± 3521	14.11 ± 0.05	5.96 ± 0.09	131.6 ± 4.5	4.79 ± 0.03	18.15 ± 0.30	25.8 ± 0.9
4661	91644 ± 3379	13.83 ± 0.05	6.09 ± 0.10	123.8 ± 4.2	4.59 ± 0.03	16.36 ± 0.29	23.7 ± 0.8
4682	278621 ± 9738	13.43 ± 0.04	6.06 ± 0.07	365.4 ± 12.5	4.86 ± 0.02	20.28 ± 0.22	76.5 ± 2.6
4700	84348 ± 3266	13.21 ± 0.05	6.27 ± 0.10	108.8 ± 3.7	4.39 ± 0.03	16.30 ± 0.29	20.9 ± 0.7
4740	19845 ± 1052	13.20 ± 0.08	6.98 ± 0.17	25.6 ± 0.9	4.36 ± 0.05	15.66 ± 0.46	4.9 ± 0.2
4750	45086 ± 1846	12.58 ± 0.08	6.59 ± 0.17	55.4 ± 1.9	4.62 ± 0.05	16.80 ± 0.46	11.8 ± 0.4
4781	61428 ± 2426	12.90 ± 0.05	6.37 ± 0.10	77.4 ± 2.6	4.76 ± 0.03	18.19 ± 0.30	16.5 ± 0.6
4843	45426 ± 1866	12.12 ± 0.05	6.82 ± 0.11	53.8 ± 1.8	4.56 ± 0.03	16.92 ± 0.29	11.7 ± 0.4

Systematic uncertainties in the BF measurement

The sources of systematic uncertainties are summarized in Table VI; their sum in quadrature is taken as the total systematic uncertainty.

TABLE VI. Systematic uncertainties in the BF measurement.

Sources	$\mathcal{B}(\Lambda_c^+ \rightarrow \Lambda\pi^+\eta)(\%)$
Tracking	0.9
PID	0.3
Λ reconstruction	2.6
η reconstruction	1.0
BDTG cut	1.1
Signal model	2.7
Fit model	0.9
$\mathcal{B}_{\text{inter}}$	0.9
$N_{\Lambda_c^+ \bar{\Lambda}_c^-}$	3.9
MC statistics	0.4
Total	5.7

- *Tracking, PID, Λ and η reconstruction.* We use $J/\psi \rightarrow p\bar{p}\pi^+\pi^-$ control samples to determine the pion tracking efficiency, $J/\psi \rightarrow \bar{p}K^+\Lambda, pK^-\bar{\Lambda}$ to determine the Λ reconstruction efficiency, and $\psi(3686) \rightarrow J/\psi\pi^0\pi^0$ and $e^+e^- \rightarrow \omega\pi^0$ control samples to determine the η reconstruction efficiency. The detection efficiency is re-weighted, and an alternative simultaneous fit is performed. The difference between the nominal and alternative fit results is taken as the uncertainty.

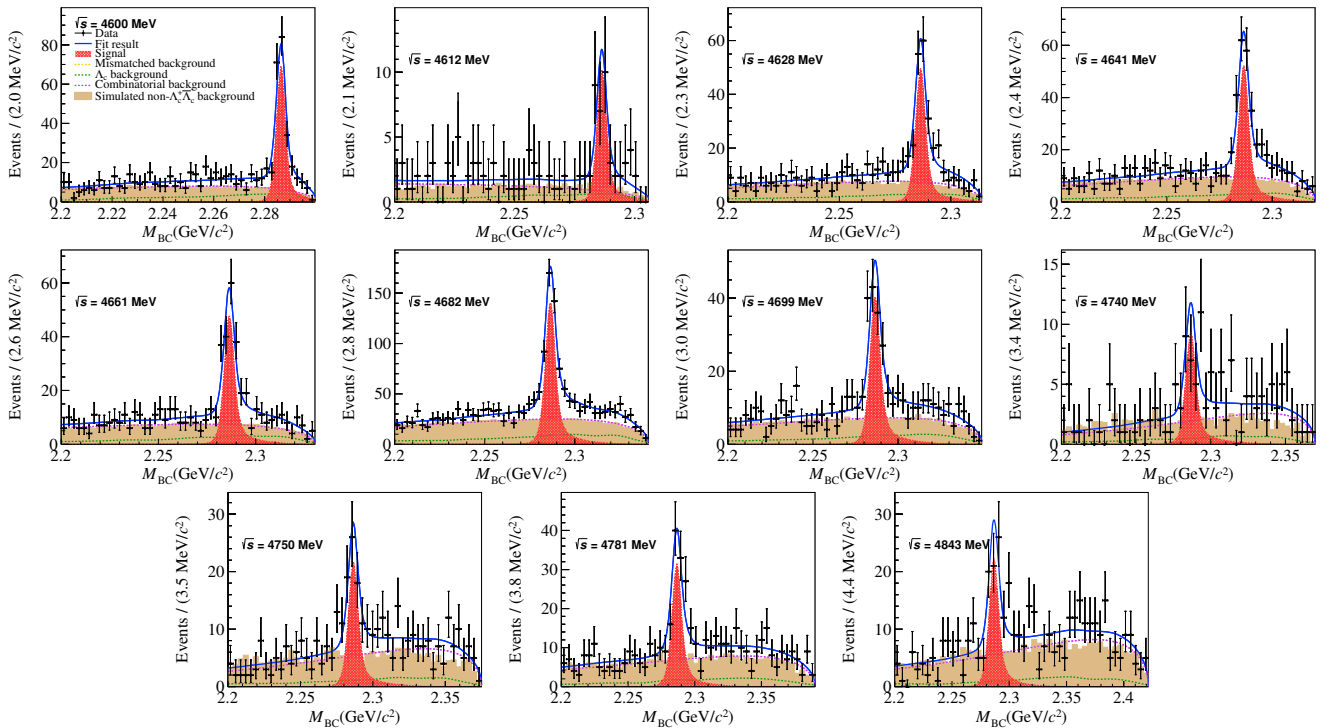


FIG. 8. The simultaneous fit to the M_{BC} distributions combined from the $\eta \rightarrow \gamma\gamma$ and $\eta \rightarrow \pi^+\pi^-\pi^0$ channels at different energy points. The points with error bars are data, the brown solid histograms are MC-simulated background derived from the inclusive MC sample excluding $\Lambda_c^+\bar{\Lambda}_c^-$, the red grid histograms are signal, the orange dashed lines are mismatched background, the green dashed lines are Λ_c decay background, the violet dashed lines are combinatorial background shapes, and the blue lines are total fit curves.

- *BDTG cut.* The systematic uncertainty due to the BDTG cut is studied with a $\Lambda_c^+ \rightarrow \Lambda\pi^+\pi^0$ control sample. The difference between the BF before applying the BDTG cut and that after the cut, 1.1%, is assigned as the systematic uncertainty.
- *Signal model.* The systematic uncertainty due to signal model is assigned to be 2.7%, by varying the amplitude analysis model parameters according to the error matrix and re-weighting the detection efficiency.
- *Fit model.* To estimate the systematic uncertainty due to the fit model, we re-weight the signal shape according to the error matrix and also vary the fixed background numbers by $\pm 1\sigma$. The quadrature sum of the difference between nominal and alternative fit results, 0.9%, is taken as the uncertainty.
- $\mathcal{B}_{\text{inter}}$. The systematic uncertainty due to the $\mathcal{B}_{\text{inter}}$ factor is estimated by varying it by $\pm 1\sigma$ [8]. The deviation from the nominal fit result, 0.9%, is assigned as the systematic uncertainty.
- $N_{\Lambda_c^+\bar{\Lambda}_c^-}$. The systematic uncertainty due to $N_{\Lambda_c^+\bar{\Lambda}_c^-}$ is estimated by varying this yield by $\pm 1\sigma$. The change of the fit result, 3.9%, is taken as the systematic uncertainty.
- *MC statistics.* The uncertainty related to MC statistics is estimated by varying the detection efficiencies by $\pm 1\sigma$. The change of the nominal fit result, 0.4%, is taken as the systematic uncertainty.

- [6] S. M. Flatté, *Phys. Lett. B* **63**, 224 (1976).
- [7] M. Ablikim *et al.* (BESIII Collaboration), *Phys. Rev. D* **95**, 032002 (2017).
- [8] R.L. Workman *et al.* (Particle Data Group), *Prog. Theor. Exp. Phys.* **2022**, 083C01 (2022) and 2023 update.
- [9] A. V. Sarantsev, M. Matveev, V. A. Nikonov, A. V. Anisovich, U. Thoma and E. Klempt, *Eur. Phys. J. A* **55**, 180 (2019).
- [10] M. Ablikim *et al.* (BESIII Collaboration), *Phys. Rev. D* **99**, 032010 (2019).
- [11] M. Wang, Y. Jiang, Y. Liu, W. Qian, X. Lyu and L. Zhang, *Chin. Phys. C* **45**, 063103 (2021).
- [12] H. Chen and R. G. Ping, *Phys. Rev. D* **99**, 114027 (2019).
- [13] M. Ablikim *et al.* (BESIII Collaboration), *Phys. Rev. Lett.* **120**, 132001 (2018).
- [14] M. Ablikim *et al.* (BESIII Collaboration), *Phys. Rev. Lett.* **131**, 191901 (2023).
- [15] G. Y. Wang, N. C. Wei, H. M. Yang, E. Wang, L. S. Geng and J. J. Xie, *Phys. Rev. D* **106**, 056001 (2022).